Mineralogical Magazine (2020), **84**, 568–583
doi:10.1180/mgm.2020.57

CAMBRIDGE UNIVERSITY PRESS

Article

Crystal chemistry of the variscite and metavariscite groups: Crystal structures of synthetic $CrAsO_4 \cdot 2H_2O$, $TlPO_4 \cdot 2H_2O$, $MnSeO_4 \cdot 2H_2O$, $CdSeO_4 \cdot 2H_2O$ and natural bonacinaite, $ScAsO_4 \cdot 2H_2O$

Uwe Kolitsch[1,2*], Matthias Weil[3], Vadim M. Kovrugin[4,5] and Sergey V. Krivovichev[4,6]

[1]Mineralogisch-Petrographische Abt., Naturhistorisches Museum, Burgring 7, A-1010 Wien, Austria; [2]Institut für Mineralogie und Kristallographie, Universität Wien, Althanstrasse 14, A-1090 Wien, Austria; [3]Institut für Chemische Technologien und Analytik, Bereich Strukturchemie, Technische Universität Wien, Getreidemarkt 9/164-SC, A-1060 Wien, Austria; [4]Department of Crystallography, Institute of Earth Sciences, St. Petersburg State University, 199034 St. Petersburg, Russia; [5]ICMCB-CNRS, Université de Bordeaux, Bordeaux INP, UMR 5026, 33600 Pessac Cedex, France; and [6]Nanomaterials Research Center, Kola Science Center, Russian Academy of Sciences, Fersmana 14, 184209 Apatity, Russia

Abstract

We report the crystal structures of four synthetic members of the variscite group (space group type *Pbca*) and of bonacinaite, the first naturally occurring scandium arsenate member of the metavariscite group. All structures were determined using single-crystal X-ray intensity data. The following members were all synthesised under either mild hydrothermal conditions or by wet-chemical methods (<90°C). $CrAsO_4 \cdot 2H_2O$ (deep green): $a = 8.894(2)$, $b = 9.946(2)$, $c = 10.206(2)$ Å and $V = 902.8(3)$ Å^3; $R_1 = 2.14\%$. $Tl^{3+}PO_4 \cdot 2H_2O$ (colourless): $a = 10.2848(7)$, $b = 8.8578(6)$, $c = 10.3637(7)$ Å and $V = 944.14(11)$ Å^3 (data at –173°C); $R_1 = 2.56\%$. $MnSeO_4 \cdot 2H_2O$ (pale pink): $a = 10.441(2)$, $b = 9.2410(18)$, $c = 10.552(2)$ Å and $V = 1018.1(3)$ Å^3; $R_1 = 2.19\%$. A different method of preparation of $MnSeO_4 \cdot 2H_2O$ yielded crystals with very similar unit-cell parameters, $a = 10.4353(5)$, $b = 9.2420(5)$ and $c = 10.5349(6)$ Å; $R_1 = 2.25\%$. $CdSeO_4 \cdot 2H_2O$ (colourless) has $a = 10.481(1)$, $b = 9.416(1)$, $c = 10.755(1)$ Å and $V = 1061.4(2)$ Å^3; $R_1 = 1.53\%$. The thermal behaviour of the two selenate members was studied by a combination of DSC and TG, supplemented by PXRD. Bonacinaite (IMA2018-056), metavariscite-type natural $(Sc,Al)(As,P)O_4 \cdot 2H_2O$ (ideally $ScAsO_4 \cdot 2H_2O$), crystallises in the space group $P2_1/n$, with $a = 5.533(1)$, $b = 10.409(2)$, $c = 9.036(2)$ Å, $\beta = 91.94(3)°$ and $V = 520.11(18)$ Å^3; $R_1 = 3.66\%$. The structural formula, supported by chemical analysis, is $(Sc_{0.807(1)}Al_{0.193})(As_{0.767(7)}P_{0.233})O_4 \cdot 2H_2O$. All structures are based on frameworks built by corner-sharing of TO_4 tetrahedra ($T = P^{5+}$, As^{5+} or Se^{6+}) with $MO_4(H_2O)_2$ ($M = Mn^{2+}$, Cd^{2+}, Cr^{3+}, Sc^{3+} or Tl^{3+}) octahedra. The flexible frameworks are reinforced by partly bifurcated, strong to weak hydrogen bonds.

The crystal chemistry of all known synthetic and natural members of the variscite and metavariscite groups is discussed and compared, and the relative stabilities are evaluated. With the aid of the *COMPSTRU* program (Bilbao Crystallographic Server), a quantitative comparison of the crystal structures in both groups is given. Calculations of the structural and topological complexity reveal that the metavariscite structure type is structurally and topologically simpler than that of variscite. It is suggested that metavariscite and phosphosiderite are metastable kinetically stabilised phases, in contrast to thermodynamically stable variscite and strengite, respectively. The 3D frameworks of the members of both groups have been shown to be potential electrode materials for rechargeable Li ion batteries.

Keywords: chromium arsenate dihydrate, scandium arsenate dihydrate, thallium(III) phosphate dihydrate, manganese selenate dihydrate, cadmium selenate dihydrate, crystal structure, variscite group, metavariscite group, crystal chemistry, stability, structural complexity, electrode materials, Li ion batteries

(Received 23 May 2020; accepted 2 July 2020; Accepted Manuscript published online: 8 July 2020; Associate Editor: Oleg I Siidra)

Introduction and previous work

Since the first determinations of the crystal structures of variscite (orthorhombic $AlPO_4 \cdot 2H_2O$, *Pbca*) and topologically related metavariscite (monoclinic dimorph, $P2_1/n$) by Kniep *et al.* (1977) and Kniep and Mootz (1973) (redetermination, correcting a previous study of Fayos and Salvador-Salvador, 1971), respectively, a large number of both naturally occurring and synthetic members of these two groups have been reported. These members comprise predominantly phosphates and arsenates, but also vanadates (only one representative) and selenates (three representatives). An up-to-date compilation of the known minerals and synthetic compounds and their crystal data is provided in Tables 1 and 2 (variscite- and metavariscite-types, respectively), along with footnotes pointing out some errors and inconsistencies in the published data. This compilation reveals an interesting observation: while there are six variscite-type arsenate members, the metavariscite-type members include only one arsenate member ($ScAsO_4 \cdot 2H_2O$). The topology of the framework-based variscite and metavariscite structure types was elucidated recently by Ilyushin and Blatov (2017), who also discussed the functional

***Author for correspondence:** Uwe Kolitsch, Email: uwe.kolitsch@nhm-wien.ac.at
Cite this article: Kolitsch U., Weil M., Kovrugin V.M. and Krivovichev S.V. (2020) Crystal chemistry of the variscite and metavariscite groups: Crystal structures of synthetic $CrAsO_4 \cdot 2H_2O$, $TlPO_4 \cdot 2H_2O$, $MnSeO_4 \cdot 2H_2O$, $CdSeO_4 \cdot 2H_2O$ and natural bonacinaite, $ScAsO_4 \cdot 2H_2O$. *Mineralogical Magazine* **84**, 568–583. https://doi.org/10.1180/mgm.2020.57

Table 1. Overview on variscite-type minerals and synthetic compounds (five phosphates, five arsenates, three selenates).

Mineral/Compound	Space group	*a* (Å)	*b* (Å)	*c* (Å)	*V* (Å^3)	Reference
Variscite, $AlPO_4·2H_2O$	*Pbca*	9.822(3)	8.561(3)	9.630(3)	809.7	Kniep *et al.* (1977)
	Pbca	9.821	8.558	9.622	808.81	ICDD-PDF 33-33
	Pcab	9.83	8.56	9.64	811.2	Salvador Salvador and Fayos (1972), ICDD-PDF 25-19
Strengite, $FePO_4·2H_2O$	*Pbca*	8.720(1)	9.879(1)	10.119(2)	871.7(3)	Kolitsch (unpublished SXRD refinement)
	Pbca	8.722(3)	9.878(2)	10.1187(14)	876.8	Taxer and Bartl (2004)
(syn.)	*Pbca*	9.8674(11)	10.0973(11)	8.7046(10)	867.27(17)	Song *et al.* (2002b)
	Pcab	10.12	9.886	8.723	872.91	ICDD-PDF 33-667
	Pcab	10.05	9.92	8.74	871.3	Arlidge *et al.* (1963); ICDD-PDF 15-513
(Al-rich)	*Pcab*	9.99	9.78	8.66	846.1	Arlidge *et al.* (1963); ICDD-PDF 15-391
	Pcab	8.65	10.05	9.80	851.9	Kleber and Weiner (1958)
	n.d.	8.65	10.06	9.84	856.3	Kokkoros (1939)
$GaPO_4·2H_2O$	*Pbca*	9.9260(1)	8.6189(1)	9.7622(1)	835.17	Loiseau *et al.* (1998)
$InPO_4·2H_2O$	*Pbca*	10.36	8.84	10.19	933.2	Mooney-Slater (1961)
	Pbca	8.842(2)	10.1870(10)	10.327(2)	930.19	Xu *et al.* (1995)
$TlPO_4·2H_2O$	*Pbca*	10.39	8.87	10.31	950.2	Mooney-Slater (1961)
(at −173°C)	*Pbca*	10.2848(7)	8.8578(6)	10.3637(7)	944.14(11)	This work
Mansfieldite, $AlAsO_4·2H_2O$ (syn.)	*Pbca*	8.8218(5)	9.8252(6)	10.1163(6)	876.8(2)	Harrison (2000)
Mansfieldite (Co-bearing), $(Al_{0.95}Co_{0.05})AsO_4·2H_2O$[1)]	*Pbca*	8.79263(11)	9.79795(10)	10.08393(11)	868.728(16)	Zoppi and Pratesi (2009)
Scorodite, $FeAsO_4·2H_2O$	*Pcab*	8.937(1)	10.278(2)	9.996(2)	918.2	Hawthorne (1976)
	Pbca	10.325(6)	8.953(3)	10.038(2)	927.9	Kitahama *et al.* (1975)
	Pbca	8.942(7)	10.339(8)	10.075(8)	931.4	Xu *et al.* (2007)
$CrAsO_4·2H_2O$	*Pcab*	10.207	9.934	8.884	900.8	Ronis (1970); Ronis and D'Yvoire (1974)
	Pbca	8.894(2)	9.946(2)	10.206(2)	902.8(3)	This work
Yanomamite, $InAsO_4·2H_2O$	*Pbca*	10.446(6)	9.085(4)	10.345(6)	981.8(7)	Botelho *et al.* (1994)
(syn.)	*Pbca*	10.471(3)	9.092(2)	10.341(2)	984.5(5)	Botelho *et al.* (1994)
(syn.)	*Pbca*	10.478(1)	9.0998(8)	10.345(1)	986.4	Tang *et al.* (2002)
(syn.)	*Pbca*	10.468(4)	9.090(4)	10.344(4)	984.3	Chen *et al.* (2002)
(syn.)	*Pbca*	10.40(4)	9.05(4)	10.24(4)	963.8	Le Berre *et al.* (2007)
$GaAsO_4·2H_2O$	*Pbca*	10.160(1)	8.862(1)	9.941(1)	895.0(2)	Dick (1997)
	Pbca	10.16(4)	8.85(4)	9.92(4)	892.0	Le Berre *et al.* (2007)
	Pbca	8.8574(4)	9.9347(4)	10.1625(2)	894.25(5)	Spencer *et al.* (2015)
	Pbca	9.099(4)	10.344(5)	10.476(5)	986	ICDD-PDF 54-309[2)]
$TlAsO_4·2H_2O$	*Pbca*	10.48	9.16	10.49	1007.0	Mooney-Slater (1961)
(at −173°C)	*Pbca*	10.4658(10)	9.1272(9)	10.5106(10)	1004.01(17)	Schroffenegger *et al.* (2019)
$MgSeO_4·2H_2O$	n.d.	10.304(1)	10.351(9)	9.138(9)	974.6	Stoilova and Koleva (1995*a*,*b*)
$MnSeO_4·2H_2O$[3)]	n.d.	10.47	9.24	10.51	1017	Kokkoros (1939)
	Pbca	10.441(2)	9.2410(18)	10.552(2)	1018.1(3)	This work
	Pbca	10.4353(5)	9.2420(5)	10.5349(6)	1016.02(9)	Kovrugin *et al.* (2016), this work
$CoSeO_4·2H_2O$	n.d.	n.d.	n.d.	n.d.	n.d.	Maier *et al.* (1965), Nabar and Paralkar (1975), Koleva and Stoilova (1997)
$NiSeO_4·2H_2O$	n.d.	10.351(4)	10.219(4)	9.017(5)	953.9(6)	Stoilova and Koleva (1997)
$ZnSeO_4·2H_2O$	*Pbca*	9.0411(13)	10.246(2)	10.3318(15)	957.1(3)	Krivovichev (2007)
$CdSeO_4·2H_2O$	n.d.	10.42	9.36	10.71	1045	Kokkoros (1939)
	Pbca	10.481(1)	9.416(1)	10.755(1)	1061.4(2)	This work

Notes: n.d. = not determined. Space groups are those given in the cited literature, some settings appear doubtful, although two different *Pbca* settings exist. A closely related, metastable species is parascorodite, trigonal $FeAsO_4·2H_2O$ (space group $P\bar{3}c1$; Perchiazzi *et al.*, 2004).
[1)]Simplified; formula given by Zoppi and Pratesi (2009) is: $(Al_{0.944}Co^{3+}_{0.046}Cu^{2+}_{0.005}Fe^{3+}_{0.003}Zn^{2+}_{0.002})_{\Sigma=1}(As_{0.972}Al_{0.022}P_{0.006})_{\Sigma=1}O_{3.975}·2H_2O$ (*sic!*).
[2)]The unit-cell parameters given in ICDD-PDF 54-309 (Wang, S.-L., Grant-in-Aid, 2002) appears to be those of $InAsO_4·2H_2O$, not of $GaAsO_4·2H_2O$; the sample was "prepared at 160°C for 72 h".
[3)]$MnSeO_4·2H_2O$ is also reported by Koleva and Stoilova (1999), but without unit-cell parameters.

role of the hydrogen bonds within the frameworks (see also the discussion of topological features below).

The aim of the present article is threefold. Firstly, we present the hydrothermal synthesis and crystal structures of four members of the variscite group, *viz.* the arsenate $CrAsO_4·2H_2O$, the phosphate $Tl^{3+}PO_4·2H_2O$ and the two selenates $Mn^{2+}SeO_4·2H_2O$ and $CdSeO_4·2H_2O$. In addition, the thermal behaviours of the two selenates are reported. For all compounds, only unit-cell parameters were previously available (Table 1).

The existence of $CrAsO_4·2H_2O$ was first reported by Lukaszewski *et al.* (1961) in a study of the aqueous system Cr(III)–arsenic acid. The dihydrate, obtained from dehydration of the hexahydrate (in two steps at 0°C and 50°C, with the intermediate formation of a tetrahydrate), was found to be stable up to 120°C. Subsequently, $CrAsO_4·2H_2O$ was also reported by Ronis (1970) and Ronis and D'Yvoire (1974) who synthesised the compound by heating a solution of $Cr(H_2AsO_4)_3·5H_2O$ and H_3AsO_4 at 270°C in a sealed container and by double decomposition of the appropriate metal salts with H_3AsO_4 or by hydrolysis of $Cr(H_2AsO_4)_3$, respectively. On the basis of an indexed powder X-ray diffraction (PXRD) pattern, these authors suggested that $CrAsO_4·2H_2O$ is isotypic with variscite, and provided the following unit-cell parameters for space group *Pcab* (non-standard setting of the space group no. 61): $a = 10.207$, $b = 9.934$, $c = 8.884$ Å and $V = 900.8$ Å^3. The two selenates, first reported by Kokkoros (1939), were synthesised independently by two groups among

https://doi.org/10.1180/mgm.2020.57 Published online by Cambridge University Press

Table 2. Overview on metavariscite-type minerals and synthetic compounds (seven phosphates and one arsenate).

Mineral/Compound	Space group	*a* (Å)	*b* (Å)	*c* (Å)	β (°)	*V* (Å^3)	Ref.
Metavariscite, $AlPO_4·2H_2O$	$P2_1/n$	5.178(2)	9.514(2)	8.454(2)	90.35(2)	416.5	Kniep and Mootz (1973)
	$P2_1/n$	5.14(3)	9.45(5)	8.45(5)	90	410	Borensztajn (1965, 1966)
	$P2_1/n$	5.182	9.507	8.448	90.4	416.2	Fayos and Salvador-Salvador (1971)
	$P2_1/n$	5.189(6)	9.52(2)	8.465(7)	90.5(3)	418.1(11)	Elton (1996)
Kolbeckite, $ScPO_4·2H_2O$ (syn.)	$P2_1/n$	5.4429(8)	10.2513(15)	8.9094(11)	90.253(7)	497.11	Bull *et al.* (2003)
(natural)	$P2_1/n$	5.4258(4)	10.2027(8)	8.9074(7)	90.502(5)	493.08(7)	Yang *et al.* (2007)
Phosphosiderite, $FePO_4·2H_2O$	$P2_1/n$	5.32(3)	9.75(5)	8.65(5)	90.6	449	Borensztajn (1966)
	$P2_1/n$	5.330(3)	9.809(4)	8.714(5)	90.60(13)	455.6	Fanfani and Zanazzi (1966)
	$P2_1/n$	5.30	9.77	8.73	90.6	452	Moore (1966)
(syn.)	$P2_1/n$	5.3071(10)	9.7548(19)	8.6752(16)	90.163(4)	449.11(15)	Song *et al.* (2002b)
(syn.)	$P2_1/n$	5.335(5)	9.808(12)	8.720(7)	90.54(5)	456.3(8)	Taxer and Bartl (2004)
(As-bearing, syn.), $Fe(P_{0.98}As_{0.02})O_4·2H_2O$	$P2_1/n$	5.329(11)	9.797(2)	8.7140(17)	90.57(3)	454.9	Bolanz *et al.* (2016)
$VPO_4·2H_2O$	$P2_1/n$	5.3112(2)	9.8447(2)	8.6536(2)	91.23(1)	452.37	Schindler *et al.* (1995)
$GaPO_4·2H_2O$	$P2_1/n$[1)]						Mooney-Slater (1966)
$InPO_4·2H_2O$	$P2_1/n$	5.4508(12)	10.2229(12)	8.8830(17)	91.50(2)	494.82	Sugiyama *et al.* (1999)
	$P2_1/n$	5.4551(3)	10.2293(4)	8.8861(3)	91.489(4)	495.69	Tang *et al.* (2002)
Bonacinaite, ideally $ScAsO_4·2H_2O$	$P2_1/n$	5.533(1)	10.409(2)	9.036(2)	91.94(3)	520.11(18)	Barresi *et al.* (2005), this work
$ScAsO_4·2H_2O$	n.d.[2)]	5.64(5)	10.47(1)	9.36(1)	~90	~553	Komissarova *et al.* (1971)

Note: Some unit-cell volumes were not given in the original publication and were therefore calculated from the published unit-cell parameters.
[1)]For $GaPO_4·2H_2O$, Mooney-Slater (1966) gives an incorrect cell with $a = 9.77$, $b = 9.64$, $c = 9.68$ Å and $\beta = 102.7°$, and a doubtful interpretation of the crystal structure.
[2)]n.d. – not determined. Komissarova *et al.* (1971) state that synthetic $ScAsO_4·2H_2O$ has a "monoclinically distorted rhombic lattice"; see also Carron *et al.* (1958), Ivanov-Emin *et al.* (1971) and Komissarova *et al.* (1973).

the present authors. A brief, preliminary report on $MnSeO_4·2H_2O$ has already been presented at a conference (Kovrugin *et al.*, 2016).

The second aim of the present paper is to present the crystal structure of bonacinaite (IMA2018-056; Cámara *et al.*, 2018), natural metavariscite-type $(Sc,Al)(As,P)O_4·2H_2O$ from the abandoned Varenche mine, Saint-Barthélemy, Nus, Valle d'Aosta, Italy, from which it was briefly described by Barresi *et al.* (2005), including the reporting of the unit-cell parameters and space-group symmetry, based on a crystal-structure determination of U.K., the second author of the mentioned paper. The Varenche mine worked on a metamorphic manganese deposit containing a number of rare As and V minerals, as well as the scandium silicate thortveitite (Barresi *et al.*, 2005). Bonacinaite forms tiny colourless (partly pale violet due to a violet ring-like zone in the centre), tabular crystals that show a pseudohexagonal outline, have glassy lustre and are transparent. They sit in a small void of a matrix composed of granular braunite, quartz and manganese oxides, and are associated with corroded arseniopleite nearby the void.

Synthetic $ScAsO_4·2H_2O$ is known and was reported for the first time by Carron *et al.* (1958) who, in a study on $REEXO_4$ (X = P, As or V) compounds, also prepared a "hydrated scandium arsenate from solutions of $ScCl_3$ and dilute arsenic acid which was isostructural with the metavariscite group of minerals." No crystal data or indexed powder diffraction pattern were given. Subsequently, $ScAsO_4·2H_2O$ was also observed in a study of the system $ScCl_3$–Na_2HAsO_4–H_2O at 200°C by Ivanov-Emin *et al.* (1971). These authors synthesised the compound by reaction of a freshly prepared $Sc(OH)_3$ solution with H_3AsO_4 at 25°C. Komissarova *et al.* (1971) prepared $ScAsO_4·2H_2O$ as a white crystalline powder from aqueous solutions at the As/Sc ratios of 0.45–3.9 and pH 2.0–7.1. They did not determine the compound's space-group symmetry, but suggested a "monoclinically distorted rhombic lattice", with $a = 5.64(5)$, $b = 10.47(1)$, $c = 9.36(1)$ Å, $\beta \approx 90$ and $V \approx 553$ Å^3. Komissarova *et al.* (1973) reported infrared and nuclear magnetic resonance spectra of $ScAsO_4·2H_2O$ and its solubility in some acids and bases.

The third aim of our study is to discuss the crystal chemistry and structural topology of the variscite and metavariscite groups on the basis of a comparison of standardised structure data, an attempt which has never been made so far. It is worth pointing out that many of the data on the members of these groups are reported with respect to the non-standard space-group setting *Pcab*, as the *a* and *c* unit-cell parameters in the variscite group are very similar and the convention *a*>*b*>*c* was usually followed. Furthermore, the relative thermodynamic stabilities of the members of both groups and their structural and topological complexities are evaluated. We also provide an insight into the possible application of selected members as electrode materials.

Experimental

Syntheses

$CrAsO_4·2H_2O$ was synthesised as part of a larger project with the aim of an extensive study of the insufficiently known system M^{1+}–M^{3+}–As–O–H (M^{1+} = Li, Na, K, Rb, Cs, Ag, Tl or NH_4; M^{3+} = Al, Ga, In, Sc, Cr or Fe) (e.g. Schwendtner and Kolitsch, 2007*a*,*b*, 2017, 2018, and references cited therein). $CrAsO_4·2H_2O$ was prepared by mild hydrothermal methods in Teflon-lined stainless steel autoclaves (T = 220°C, duration 7 days with slow furnace cooling) from a mixture of reagent-grade $Sr(OH)_2·8H_2O$, $Cr(NO_3)_3·9H_2O$, $H_3AsO_4·0.5H_2O$ (volume ratio ~1:1:3) and distilled water. The Teflon container was filled up with distilled water to ~70–80% of its inner volume. Initial and final pH values were ~0.5 and <~0.5, respectively. The reaction products were filtered and washed with distilled water. They contained deep green, tabular crystals with a maximum dimension of ~0.07 mm and a habit equivalent to that of strengite (i.e. with sword-shaped crystal terminations). $CrAsO_4·2H_2O$ was also obtained as tiny green crystals from a hydrothermal run containing a mixture of reagent-grade PbO, $Cr(NO_3)_3·9H_2O$, $H_3AsO_4·0.5H_2O$ and GeO_2. Initial pH was <~0.5; after the run, the reaction products were nearly dry. These $CrAsO_4·2H_2O$ crystals were associated with an uninvestigated greyish grainy material. The observation of Lukaszewski *et al.* (1961) that $CrAsO_4·2H_2O$ is only stable below 120°C, suggests that in both hydrothermal runs the compound crystallised during furnace-cooling.

https://doi.org/10.1180/mgm.2020.57 Published online by Cambridge University Press

Synthesis and crystal growth of $Tl^{3+}PO_4{\cdot}2H_2O$ was performed according to the method of Mooney-Slater (1961): 1 g Tl_2O_3 was dissolved in boiling concentrated nitric acid (5 ml). The slightly opaque solution was then filtered warm through a glass frit and cooled down to room temperature. Concentrated phosphoric acid was added dropwise (altogether 2 ml) to the colourless solution. Then water was added to the still clear solution until clouding. The reaction mixture was subsequently heated to ~80°C for two hours. In that time, a cloudy greyish precipitate with an amorphous appearance formed. The mixture was then stored at a warm place (40°C) for three weeks and was allowed to slowly evaporate. Colourless crystals had formed from the precipitate with the typical form as snubbed bipyramids with maximum edge lengths of 0.3 mm.

The preparation of $MnSeO_4{\cdot}2H_2O$ was achieved by two different methods. In method 1, an excess of $MnCO_3$ was dissolved in hot diluted H_2SeO_4 (Merck, p.A.). The resulting solution was then filtered from the remaining solid and concentrated on a water bath (90°C). After evaporation at ~60°C, pale pink single crystals of $MnSeO_4{\cdot}2H_2O$ with an unspecific form were picked out of the hot solution and enclosed in "magic oil" (low-viscous perfluoropolyether 216, Riedel de Haën). This was necessary because the crystals were found to be sensitive towards moisture and to decompose under inclusion of water. When the solution was allowed to cool down to room temperature, crystals exclusively of $MnSeO_4{\cdot}5H_2O$ (Euler *et al.*, 2003) had formed.

In method 2, an aqueous solution of hydrated manganese(II) chloride (2.4 mmol), 40% selenic acid (4.7 mmol) and distilled water (10 ml) was used. The solution was stirred with a magnetic stirrer at 80°C for three hours until it became fully homogeneous. Then the solution was poured onto a watch glass and left in a fume hood to evaporate at room temperature. Single crystals of $MnSeO_4{\cdot}2H_2O$ suitable for single-crystal X-ray diffraction analysis appeared at the bottom of the watch glass after two days.

Preparation of $CdSeO_4{\cdot}2H_2O$ was as follows: CdO (Merck, p.A.) was dissolved in a diluted H_2SeO_4 (Merck, p.A.) solution in excess. After evaporation at room temperature, the resulting $CdSeO_4{\cdot}2H_2O$ crystals were recrystallised in demineralised water. Colourless translucent crystals with mostly plate-like forms and an edge-length of up to 1 mm were then obtained from the cooled solution. The crystals are non-sensitive towards moisture and are stable at room temperature. We note, however, that in an old study of the system $CdSeO_4$–H_2O (Klein, 1940), $CdSeO_4{\cdot}2H_2O$ is considered a metastable phase above –11.0°C.

Single-crystal X-ray diffraction

Selected crystals of $CrAsO_4{\cdot}2H_2O$ and bonacinaite (ideally $ScAsO_4{\cdot}2H_2O$) were studied with a Nonius KappaCCD diffractometer equipped with a 300 µm diameter capillary-optics collimator to provide increased resolution. Intensity data collections were carried out using the parameters listed in Tables 3 and 4, respectively. The measured intensity data were processed with the Nonius program suite DENZO-SMN and corrected for Lorentz polarisation, background and absorption effects (see Table 3).

Table 3. Crystal data, data collection information and refinement details for variscite-type synthetic $CrAsO_4{\cdot}2H_2O$, $TlPO_4{\cdot}2H_2O$, $MnSeO_4{\cdot}2H_2O$ and $CdSeO_4{\cdot}2H_2O$.

Crystal data				
Empirical formula	$CrAsO_4{\cdot}2H_2O$	$TlPO_4{\cdot}2H_2O$	$MnSeO_4{\cdot}2H_2O$	$CdSeO_4{\cdot}2H_2O$
Space group	*Pbca*	*Pbca*	*Pbca*	*Pbca*
Unit-cell parameters *a*, *b*, *c* (Å)	10.206(2)	10.2848(7)	10.441(2)	10.4809(12)
	8.8940(18)	8.8578(6)	9.2410(18)	9.4160(11)
	9.946(2)	10.3637(7)	10.552(2)	10.7554(12)
V (Å^3)	902.8(3)	944.14(11)	1018.1(3)	1061.4(2)
Z	8	8	8	8
D_x (mg m^{-3})	3.339	4.719	3.052	3.647
µ (mm^{-1})	9.745	34.49	9.687	10.919
Crystal dimensions (mm)	0.02 × 0.05 × 0.07	0.15 × 0.15 × 0.15	0.10 × 0.08 × 0.02	0.14 × 0.10 × 0.04
Data collection				
Diffractometer	Nonius KappaCCD	Bruker Apex II (CCD)	Bruker Smart (CCD)	Bruker Smart (CCD)
Temperature (K)	293	100	295	295
Radiation, wavelength (Å)	Mo*K*α, 0.71073	Mo*K*α, 0.71073	Mo*K*α, 0.71073	Mo*K*α, 0.71073
θ range for data collection (°)	3.54–30.01	3.62–44.79	3.52–30.52	3.47–30.49
h, *k*, *l* ranges	±14, ±12, –13/14	±20, ±17, ±20	±14, –12/13, ±14	–13/14, ± 13, ±15
Total reflections	2423	28978	10553	10846
Unique refls. (R_{int})	1315 (0.0131)	3870 (0.0603)	1534 (0.0416)	1603 (0.0259)
Unique reflections $I > 2\sigma(I)$	1170	3042	1287	1473
Data completeness to θ_{max} (%)	100	100	99	99
Absorption correction method	Multi-scan (Otwinowski *et al.*, 2003)	*SADABS* (Sheldrick, 2002)	*SADABS* (Sheldrick, 2002)	*SADABS* (Sheldrick, 2002)
Structure refinement				
Refinement method	Full-matrix least-squares on F^2	Full-matrix least-squares on F^2	Full-matrix least-squares on F^2	Full-matrix least-squares on F^2
Weighting coefficients *a*, *b*	0.0296, 1.3254	0.0114, 2.2449	0.0223, 0.1120	0.0153, 0.6563
Extinction coefficient	0.0033(4)	0.00151(7)	0.0017(2)	0.00154(10)
Data/restraints/para-meters	1315/4/90	3870/4/87	1534/4/87	1603/4/87
R_1 [$I > 2\sigma(I)$], wR_2 [$I > 2\sigma(I)$]	0.0214, 0.0532	0.0256, 0.0426	0.0219, 0.0452	0.0153, 0.0351
R_1 all, wR_2 all	0.0264, 0.0551	0.0416, 0.0457	0.0329, 0.0482	0.0183, 0.0358
Goodness-of-fit on F^2	1.087	1.022	1.082	1.094
Largest diff. peak and hole (e^-/Å^3)	0.63, –0.91	1.88, –3.77	0.73, –0.52	0.49, –0.42

https://doi.org/10.1180/mgm.2020.57 Published online by Cambridge University Press

Table 4. Crystal data, data collection information and refinement details for metavariscite-type bonacinaite (ideally $ScAsO_4 \cdot 2H_2O$).

Crystal data	
Empirical formula	$(Sc_{0.807(1)}Al_{0.193})(As_{0.767(7)}P_{0.233})O_4 \cdot 2H_2O$
Space group	$P2_1/n$
Crystal dimensions (mm)	0.10 × 0.07 × 0.06
Unit-cell parameters	
a, *b*, *c* (Å), β (°)	5.533(1), 10.409(2), 9.036(2), 91.94(3)
V (Å^3)	520.11(18)
Z	4
D_x (mg m^{-3})	2.634
μ (mm^{-1})	6.080
Data collection	
Diffractometer	Nonius KappaCCD
Temperature (K)	293
Radiation, wavelength (Å)	Mo*K*α, 0.71073
θ range for data collection (°)	4.17–30.11
h, *k*, *l* ranges	±7, ±14, ±12
Total reflections	2822
Unique reflections (R_{int})	1470 (0.0243)
Unique reflections $I > 2\sigma(I)$	1178
Data completeness to θ_{max} (%)	96
Absorption correction method	Multi-scan (Otwinowski *et al.*, 2003)
Structure refinement	
Refinement method	Full-matrix least-squares on F^2
Weighting coefficients *a*, *b*	0.0531, 0.2852
Extinction coefficient	0.0052(18)
Data/restraints/parameters	1178/4/92
R_1 [$I > 2\sigma(I)$], wR_2 [$I > 2\sigma(I)$]	0.0366, 0.0867
R_1 all, wR_2 all	0.0540, 0.0947
Goodness-of-fit on F^2	1.054
Largest diff. peak and hole (e$^-$/Å^3)	0.57, −0.81

The crystal structure of $CrAsO_4 \cdot 2H_2O$ was solved in space group *Pbca* by direct methods (SHELXS-97; Sheldrick, 2008) and subsequent Fourier and difference Fourier syntheses, followed by full-matrix least-squares anisotropic refinement on F^2 (*SHELXL-2018/3*; Sheldrick, 2015). The structure model obtained confirmed the isotypy with variscite. All H atoms were located, and the O–H bond lengths restrained to 0.90(1) Å. Subsequently, the structure model of variscite (Kniep *et al.*, 1977) was adopted for a final refinement step which led to $R_1 = 2.14\%$.

The crystal structure of bonacinaite was solved in space group $P2_1/n$ by direct methods (*SHELXS-97*; Sheldrick, 2008). Details on data collection and refinement are given in Table 4. A full-matrix least-squares anisotropic refinement on F^2 (*SHELXL-2018/3*; Sheldrick, 2015) provided a structure model in full agreement with a metavariscite-type atomic arrangement. Based on subsequent scanning electron microscopy using energy-dispersive spectroscopic analyses of the studied crystal, which showed minor Al (and traces of Fe) and P (and traces of Si) as impurity constituents substituting for Sc and As, respectively, the occupancies of the Sc and As sites were refined taking into account these substitutions. The refinement converged at $R_1 = 3.66\%$ and showed that ~19% of the Sc site contained Al, and ~23% of the As site contained P (the trace amounts of Fe and Si were ignored).

Intensity datasets of crystals of $MnSeO_4 \cdot 2H_2O$ (prepared by method 1) and $CdSeO_4 \cdot 2H_2O$ were measured with a Bruker SMART (CCD) diffractometer, while a crystal of $MnSeO_4 \cdot 2H_2O$ (prepared by method 2) was measured with a Bruker APEX DUO diffractometer. The measurement of a $TlPO_4 \cdot 2H_2O$ crystal was done with a Bruker APEX-II diffractometer at −173°C. Using Bruker software (Bruker AXS, 1997, 1998*a*,*b*), the datasets were processed and corrected for Lorentz polarisation, background and absorption effects (for details see Table 3). For all synthetic crystals, systematic extinctions and structure factor statistics unambiguously indicated the centrosymmetric space group *Pbca*. Using the published coordinate set for variscite (Kniep *et al.*, 1977) as a starting model, the structures were refined with *SHELXL-2018/3* (Sheldrick, 2015). The positions of the hydrogen atoms were clearly discernible from difference-Fourier maps and included in the model, while restraining the O–H bond length to 0.90(1) Å. No significant deviation from unit occupancy was observed for any of the atoms in any of the structures of the synthetic variscite-group representatives (including $CrAsO_4 \cdot 2H_2O$).

The final positional and displacement parameters of all measured crystals are given in the deposited crystallographic information files deposited with the Principal Editor of *Mineralogical Magazine* and available as Supplementary material (see below). The latter include lists of observed and calculated structure factors. Selected bond lengths (including hydrogen bonds) and calculated bond-valence sums (BVSs) are presented in Tables 5, 6 and 7.

Thermal analysis

Thermoanalytical measurements of $CdSeO_4 \cdot 2H_2O$ and $MnSeO_4 \cdot 2H_2O$ were performed in an open system under a flowing N_2 atmosphere and a heating rate of 5°C/min on a Mettler–Toledo TG50 (35–800°C, corundum crucibles) and a Mettler–Toledo DSC-25 system (35–550°C, aluminium capsules). The remaining solids obtained after heating were identified by PXRD.

Results

Thermal behaviour of $CdSeO_4 \cdot 2H_2O$ and $MnSeO_4 \cdot 2H_2O$

The thermal behaviour on heating of the two synthetic variscite-type selenates is shown in Fig. 1 (TG and DSC curves). For the Cd compound the thermal dehydration follows a well-resolved two-step mechanism. In the first step, one mole H_2O is released at ~112°C (reaction 1a, see below) and in the second step at ~178°C the other mole H_2O is liberated and anhydrous $CdSeO_4$ is formed (1b). The theoretical mass loss of 12.36% is in good agreement with the experimental value of 12.1%. Above 600°C, $CdSeO_4$ starts to decompose under release of SeO_2 and O_2 into CdO (1c; PXRD-confirmed). The decomposition is completed at temperatures above 750°C.

For the Mn compound the course of the thermal dehydration is different and the corresponding reaction steps are not well resolved. Above ~140°C the selenate starts to dehydrate and both water molecules are more or less released simultaneously (2a,b). The small hump in the DSC curve at ~205°C actually indicates a second step, but this is not clearly visible in the corresponding TG curve. The theoretical mass loss of 15.40% for the complete dehydration is also in good agreement with the experimental value of 15.1%. It should be noted that the previously reported thermal decomposition reactions of the pentahydrate, $MnSeO_4 \cdot 5H_2O$, and the formed intermediate dihydrate $MnSeO_4 \cdot 2H_2O$ (Nabar and Paralkar, 1975), are different from the results of the present investigation. These authors observed a well-resolved two-step dehydration mechanism of the dihydrate with maxima at ~160°C and ~260°C, respectively. However, these observations could not be reproduced with our experimental set-up, possibly because of a different heating rate (10°C/min) and heating atmosphere (air flow) used by the authors of the 1975 paper. In agreement with the results of Nabar and Paralkar (1975), $MnSeO_4$ partly decomposes into $MnSeO_3$

https://doi.org/10.1180/mgm.2020.57 Published online by Cambridge University Press

Table 5. Selected interatomic distances (Å) and calculated bond valences (vu) for $CrAsO_4{\cdot}2H_2O$ and $Tl^{3+}PO_4{\cdot}2H_2O$.

$CrAsO_4{\cdot}2H_2O$			$Tl^{3+}PO_4{\cdot}2H_2O$.		
Cr–O4	1.9488(18)	0.538	Tl–O4	2.179(2)	0.546
Cr–O3	1.9633(18)	0.517	Tl–O2	2.2057(19)	0.518
Cr–O1	1.9750(18)	0.5	Tl–O3	2.212(2)	0.511
Cr–O2	1.9784(18)	0.496	Tl–O1	2.2146(19)	0.509
Cr–Ow2	1.9919(19)	0.477	Tl–Ow2	2.221(2)	0.502
Cr–Ow1	2.0272(19)	0.433	Tl–Ow1	2.310(2)	0.421
<Cr–O>	1.981	2.96 vu	<Tl–O>	2.224	3.01 vu
As–O2	1.6785(18)	1.279	P–O2	1.542(2)	1.228
As–O1	1.6861(18)	1.251	P–O1	1.544(2)	1.222
As–O3	1.6881(17)	1.244	P–O3	1.547(2)	1.213
As–O4	1.6885(17)	1.243	P–O4	1.548(2)	1.210
<As–O>	1.685	5.02 vu	<P–O>	1.545	4.87 vu
Hydrogen bonds	O–H···O (Å)	∠DHA (°)	Hydrogen bonds	O–H···O (Å)	∠DHA (°)
Ow1–H11···O3	2.584(3)	159(6)	Ow1–H11···O3	2.729(3)	142(5)
Ow1–H12···O2	3.226(3)	165(3)	Ow1–H12···O2	3.047(3)	147(6)
			Ow1–H12···O2w	2.989(3)	118(5)
Ow2–H21···O4[1)]	2.574(3)	150(5)	Ow2–H21···O4[3)]	2.636(3)	149(7)
Ow2–H22···O1[2)]	2.682(3)	164(4)	Ow2–H22···O1	2.581(3)	175(7)

[1)]There is an additional, long hydrogen bond: Ow2–H21···O3 at 3.225(3) Å, ∠DHA = 135(5)°.
[2)]There is an additional, long hydrogen bond: Ow2–H22···O2 at 2.996(3) Å, ∠DHA = 117(3)°.
[3)]There is an additional, long hydrogen bond: Ow2–H21···O3 at 3.079(3) Å, ∠DHA = 120(5)°.
Notes: Bond-valence calculations were done with the program *VALENCE* (Brown, 1996) and bond-valence parameters from Gagné and Hawthorne (2015); sum values are derived from unrounded bond-valence contributions. Bond-valence sums (vu) for the O atoms for $CrAsO_4{\cdot}2H_2O$ are O1: 1.75; O2: 1.78; O3: 1.86; O4: 1.78; Ow1: 0.43; Ow2: 0.48, and for $Tl^{3+}PO_4{\cdot}2H_2O$ are O1: 1.74; O2: 1.75; O3: 1.72; O4: 1.76; Ow1: 0.42; Ow2: 0.50.

Table 6. Selected interatomic distances (Å) and calculated bond valences (vu) for $MnSeO_4{\cdot}2H_2O$ (crystal method 1) and $CdSeO_4{\cdot}2H_2O$.

$MnSeO_4.2H_2O$			$CdSeO_4.2H_2O$		
Mn–O4	2.1355(17)	0.387	Cd–Ow2	2.2434(17)	0.380
Mn–Ow2	2.1415(17)	0.382	Cd–O4	2.2538(16)	0.371
Mn–O3	2.1819(17)	0.347	Cd–O1	2.2837(16)	0.346
Mn–O1	2.1899(17)	0.340	Cd–O3	2.2948(15)	0.337
Mn–Ow1	2.209(2)	0.325	Cd–Ow1	2.2984(19)	0.334
Mn–O2	2.2157(17)	0.320	Cd–O2	2.3245(15)	0.314
<Mn–O>	2.179	2.10 vu	<Cd–O>	2.283	2.08 vu
Se–O2	1.6297(17)	1.521	Se–O2	1.6355(15)	1.499
Se–O3	1.6357(17)	1.498	Se–O3	1.6383(16)	1.488
Se–O1	1.6407(17)	1.480	Se–O4	1.6392(15)	1.485
Se–O4	1.6408(16)	1.479	Se–O1	1.6431(15)	1.471
<Se–O>	1.637	5.98 vu	<Se–O>	1.639	5.94 vu
Hydrogen bonds	O–H···O (Å)	∠DHA (°)	Hydrogen bonds	O–H···O (Å)	∠DHA (°)
Ow1–H11···O3[1)]	2.859(3)	152(4)	Ow1–H11···O3[3)]	2.962(2)	105(3)
Ow1–H12···O2	3.217(3)	176(3)	Ow1–H12···O2	3.083(3)	170(4)
Ow2–H21···O4[2)]	2.737(2)	147(4)	Ow2–H21···O4[4)]	2.750(2)	143(4)
Ow2–H22···O1	2.723(3)	167(4)	Ow2–H22···O1	2.695(2)	175(4)

[1)]There is an additional, long hydrogen bond: Ow2–H11···Ow2 at 3.121(3) Å, ∠DHA = 115(3)°.
[2)]There is an additional, long hydrogen bond: Ow2–H21···O3 at 3.206(3) Å, ∠DHA = 126(3)°.
[3)]There is an additional, long hydrogen bond: Ow2–H11···Ow2 at 3.027(3) Å, ∠DHA = 173(4)°.
[4)]There is an additional, long hydrogen bond: Ow2–H21···O3 at 3.137(2) Å, ∠DHA = 125(3)°.
Notes: Bond-valence calculations were done with the program VALENCE (Brown, 1996) and bond-valence parameters from Gagné and Hawthorne (2015); sum values are derived from unrounded bond-valence contributions. Bond-valence sums (vu) for the O atoms for $MnSeO_4{\cdot}2H_2O$ are O1: 1.82; O2: 1.84; O3: 1.85; O4: 1.87; Ow1: 0.33; Ow2: 0.38, and for $CdSeO_4{\cdot}2H_2O$ are O1: 1.82; O2: 1.81; O3: 1.83; O4: 1.86; Ow1: 0.33; and Ow2: 0.38.

above 300°C, which is accompanied by a small mass loss but no DSC signal. At temperatures above 440°C, the anhydrous selenate decomposes completely and at temperatures >700°C Mn_3O_4 (synthetic hausmannite) is formed (2c) according to PXRD.

$$CdSeO_4{\cdot}2H_2O_{,s} \rightarrow CdSeO_4{\cdot}H_2O_{,s} + H_2O_{,g} \quad (1a)$$

$$CdSeO_4{\cdot}H_2O_{,s} \rightarrow CdSeO_{4,s} + H_2O_{,g} \quad (1b)$$

$$CdSeO_{4,s} \rightarrow CdO_{,s} + SeO_{2,g} + {}^1/_2O_{2,g} \quad (1c)$$

$$MnSeO_4{\cdot}2H_2O_{,s} \rightarrow MnSeO_4{\cdot}H_2O_{,s} + H_2O_{,g} \quad (2a)$$

https://doi.org/10.1180/mgm.2020.57 Published online by Cambridge University Press

Table 7. Selected interatomic distances (Å) and calculated bond valences (vu) for bonacinaite (ideally $ScAsO_4·2H_2O$) with the refined structural formula $(Sc_{0.807(1)}Al_{0.193})(As_{0.767(7)}P_{0.233})O_4·2H_2O$.

$ScAsO_4·2H_2O$		
Sc–O2	2.025(3))	0.541
Sc–O3	2.051(3)	0.510
Sc–O1	2.060(3)	0.500
Sc–O4	2.075(3)	0.483
Sc–Ow1	2.134(3)	0.423
Sc–Ow2	2.165(3)	0.395
<Sc–O>	2.085	2.85 vu
As–O2	1.648(3)	1.290
As–O3	1.655(3)	1.266
As–O1	1.656(3)	1.262
As–O4	1.666(3)	1.227
<As–O>	1.656	5.05 vu
Hydrogen bonds	O–H···O (Å)	∠DHA (°)
Ow1–H11···O1[1)]	2.644(4)	149(7)
Ow1–H12···O4	2.750(4)	162(4)
Ow2–H21···O3	2.810(4)	167(6)
Ow2–H22···O2[2)]	2.813(4)	143(5)

[1)]There is an additional, long hydrogen bond: Ow1–H11···O3 at 3.258(4) Å, ∠DHA = 123(5)°. [2)]There is an additional, long hydrogen bond: Ow2–H22···O1 at 3.152(4) Å, ∠DHA =122(5)°. Notes: Bond-valence calculations were done with the program *VALENCE* (Brown, 1996) and bond-valence parameters from Gagné and Hawthorne (2015), taking into account the refined occupancies of the mixed Sc and As sites. Sum values are derived from unrounded bond-valence contributions. Bond-valence sums (vu) for the O atoms are O1: 1.76; O2: 1.83; O3: 1.78; O4: 1.71; Ow1: 0.42; and Ow2: 0.40.

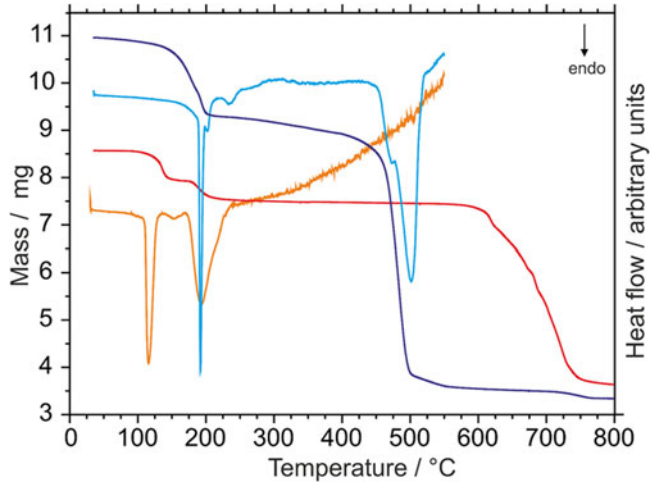

Fig. 1. Thermal analysis of $CdSeO_4·2H_2O$ (TG curve: red and DSC curve: orange) and $MnSeO_4·2H_2O$ (TG curve: dark violet and DSC curve: blue).

$$MnSeO_4·H_2O_{,s} \rightarrow MnSeO_{4,s} + H_2O_{,g} \quad (2b)$$

$$3MnSeO_{4,s} \rightarrow Mn_3O_{4,s} + 3SeO_{2,g} + O_{2,g} \quad (2c)$$

Descriptions of the structures

As the structure connectivity of the variscite and metavariscite structure types is well established, we provide only the most relevant aspects of the crystal structures. For further details, the reader is referred to dedicated previous publications (e.g. Moore, 1966; Bennett *et al.*, 1986; Taxer and Bartl, 2004; Ilyushin and Blatov, 2017).

Variscite-type synthetic compounds

The asymmetric unit of the four synthetic compounds with a variscite-type structure contains one M (M = Cr, Tl, Mn or Cd) atom, one T (T = As, P or Se) atom, six O atoms (two of which belong to water molecules) and four H atoms. The M atom is octahedrally coordinated by four O and two Ow ligands. The later are in *cis* configuration. The T atom is tetrahedrally coordinated by four O ligands. The TO_4 tetrahedra share each of their four corners with the $MO_4(H_2O)_2$ octahedra, thus forming a dense three-dimensional network. The H atoms of the two H_2O molecules point into a channel running parallel to the *a* axis, and all H atoms participate in strong to weak, partly bifurcated hydrogen bonds. The latter are stronger for the arsenate and phosphate (2.581 to 3.226 Å, Table 5) and comparatively weaker for the two selenates (2.695 to 3.217 Å, Table 6). As examples, Fig. 2 shows polyhedral representations of the structures of $CrAsO_4·2H_2O$ and $CdSeO_4·2H_2O$. Average M–O bond lengths are: $<Cr^{3+}–O>$ = 1.981 Å, $<Tl^{3+}–O>$ = 2.224 Å, <Mn–O> = 2.179 Å and <Cd–O> = 2.283 Å. The Cr value is slightly shorter than the grand mean value of 1.999 Å in inorganic compounds reported by Baur (1981). The Tl^{3+} value is very similar to that observed in the isotypic arsenate analogue $Tl^{3+}AsO_4·2H_2O$ (2.23 Å, Schroffenegger *et al.*, 2020), while the Mn value is slightly lower than the mean value of 2.205 Å given in Baur (1981). The value for Cd is comparable to those in other Cd oxysalt compounds (to our knowledge, no review on Cd–O bonds in inorganic compounds exist).

The tetrahedral anions show the following average T–O bond lengths: <As–O> = 1.685 Å, <P–O> = 1.545 Å, <Se–O> = 1.637 Å (Mn member) and 1.639 Å (Cd member). These values compare favourably with the corresponding grand mean bond lengths of 1.687(8) Å (Gagné and Hawthorne, 2018), 1.537 Å (Huminicki and Hawthorne, 2002) and 1.638 Å (Krivovichev, 2009), respectively. The slightly elevated value observed for $TlPO_4·2H_2O$ may be explained by a 'relaxation' of the structure due to the large Tl^{3+} cation and its relatively weak Tl^{3+}–O bonds, allowing the P atom to compete less strongly for the common O ligands. The O ligands O1–4 are all somewhat underbonded and, accordingly, acceptors of hydrogen bonds (see below).

The flexibility of the variscite-type framework topology is predominantly due to the corner-linkage of the three-dimensionally linked octahedral and tetrahedral building units, allowing for considerable variation of the M–O–T angles. This is also reflected in the individual distortions of the $MO_4(H_2O)_2$ octahedra, in which the sequence of O ligands with shortest *vs.* longest M–O bond varies from member to member, even when the two selenates are compared (Tables 5, 6). Moreover, the length of individual, topologically more or less equivalent hydrogen bonds, also shows distinct variation (Tables 5, 6). Bifurcation of hydrogen bonds may be present or absent. The comparatively shortest hydrogen bonds (O···O), 2.574(3) and 2.584(3) Å, are present in $CrAsO_4·2H_2O$, although $TlPO_4·2H_2O$ has also one similarly short bond, 2.581(3) Å. In scorodite, $FeAsO_4·2H_2O$, the two shortest hydrogen bonds are 2.603(9) and 2.639(9) Å according to Hawthorne (1976), somewhat different from those given for synthetic scorodite with a notably larger unit cell (*cf.* Table 1), 2.622(4) and 2.645(5) Å. In synthetic mansfieldite, $AlAsO_4·2H_2O$, the shortest O···O donor–acceptor distances are 2.578(4) and 2.592(3) Å (Harrison, 2000), i.e. very similar to those in $CrAsO_4·2H_2O$.

https://doi.org/10.1180/mgm.2020.57 Published online by Cambridge University Press

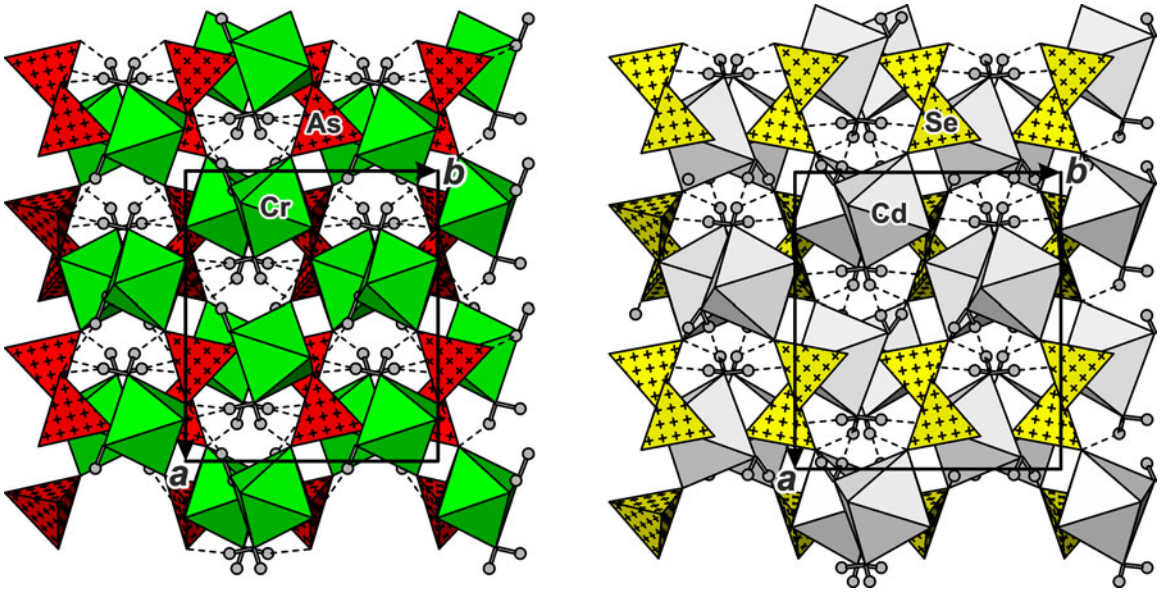

Fig. 2. Polyhedral representation of the framework crystal structures of $CrAsO_4{\cdot}2H_2O$ (left) and $CdSeO_4{\cdot}2H_2O$ (right) in a view along [001]. Hydrogen bonds are shown with dashed lines. The unit cells are outlined. All structure drawings were done with *ATOMS V. 6.3* (Dowty, 2011).

The four representatives characterised herein show that the stability range of the variscite structure type is apparently limited by the following ranges of the $^{[6]}M^{2+/3+}$ and $^{[4]}T^{5+/6+}$ cationic radii (values of Shannon, 1976): 0.535 Å (Al^{3+}) to 0.95 Å (Cd^{2+}) for $M^{2+/3+}$ ions and 0.17 Å (P^{5+}) to 0.28 Å (Se^{6+}) for $T^{5+/6+}$ ions. Therefore, we predict that the following hypothetical members may also be stable, possibly even in natural environments:

(1) The arsenates $ScAsO_4{\cdot}2H_2O$ (orthorhombic dimorph of bonacinaite, see below) and possibly $LuAsO_4{\cdot}2H_2O$. Note that hypothetical $V^{3+}AsO_4{\cdot}2H_2O$ is not considered to be stable because V^{3+} would be oxidised by the relatively strong oxidising agent As^{5+} (and, conversely, As^{5+} would be reduced by the relatively strong reducing agent V^{3+}). No compound containing both V^{3+} and As^{5+} cations is present in the current version of the Inorganic Crystal Structure Database (Belsky *et al.*, 2002), and no entry on anhydrous $V^{3+}AsO_4$ is found in any of the major literature databases.

(2) The selenates $MgSeO_4{\cdot}2H_2O$, $FeSeO_4{\cdot}2H_2O$, $CoSeO_4{\cdot}2H_2O$ and $NiSeO_4{\cdot}2H_2O$. A careful review of the literature showed that among these, $FeSeO_4{\cdot}2H_2O$ was never reported, but $CoSeO_4{\cdot}2H_2O$ was observed as an intermediate phase during the stepwise dehydration of $CoSeO_4{\cdot}4H_2O$ (Nabar and Paralkar, 1975) and $CoSeO_4{\cdot}6H_2O$ (Koleva and Stoilova, 1997). $CoSeO_4{\cdot}2H_2O$ was also reported earlier in a study of the thermodynamic properties of cobalt selenate hydrates (Maier *et al.*, 1965). Similar to its Co analogue, $NiSeO_4{\cdot}2H_2O$ was observed as a result of dehydrating $NiSeO_4{\cdot}6H_2O$ (Klein, 1940; Demassieux, 1945), of heating $NiSeO_4{\cdot}6H_2O$ at 200°C (Snyman and Pistorius, 1963), and as an intermediate phase during the stepwise dehydration of $NiSeO_4{\cdot}6H_2O$ (Stoilova and Koleva, 1997). The latter authors found that $NiSeO_4{\cdot}2H_2O$ forms orthorhombic crystals with the unit-cell parameters $a = 10.351(4)$, $b = 10.219(4)$, $c = 9.017(5)$ Å and $V = 953.9(6)$ Å^3. These values strongly suggest that the compound has in fact a variscite-type structure. $MgSeO_4{\cdot}2H_2O$ was detected on dehydrating $MgSeO_4{\cdot}6H_2O$ at 140°C (Klein, 1940). "Orthorhombic" $MgSeO_4{\cdot}2H_2O$ was observed in a study of the dehydration of $MgSeO_4{\cdot}6H_2O$, and the following unit-cell parameters were given: $a = 10.304(1)$, $b = 10.351(9)$ and $c = 9.138(9)$ (Stoilova and Koleva, 1995*a*,*b*). Again, these data serve as a strong indication that $MgSeO_4{\cdot}2H_2O$ is a variscite-type compound (Stoilova and Koleva, 1995*a*, already assumed that $MgSeO_4{\cdot}2H_2O$ is "isomorphous with $MnSeO_4{\cdot}2H_2O$", based on a comparison of PXRD data and cell parameters).

Metavariscite-type bonacinaite

The asymmetric unit of monoclinic bonacinaite contains one Sc site (with the refined occupancy $Sc_{0.807(1)}Al_{0.193}$), one As site (refined occupancy $As_{0.767(7)}P_{0.233}$), six O atoms (two of which belong to water molecules) and four H atoms, i.e. the same number of corresponding atoms as in the orthorhombic variscite-type compounds. The monoclinic angle β in bonacinaite, 91.94(3)°, is fairly close to 90°, reflecting pseudo-orthorhombic cell metrics. However, this angle β shows the largest deviation from 90° among all known metavariscite-type minerals and synthetic compounds. The structure of bonacinaite (Fig. 3) is very similar to that of the variscite-type compounds. The most notable structural difference is the orientation of the $(As,P)O_4$ tetrahedron linked to the $(Sc,Al)O_4(H_2O)_2$ octahedron and the environment of the H_2O ligands. The latter results in different hydrogen-bonding schemes.

Due to the partial substitution of Al for Sc in the $(Sc,Al)O_4(H_2O)_2$ octahedron, the mean M–O bond length, 2.085 Å (Table 7), is slightly shifted from the value expected for pure Sc compounds, 2.105 Å (Baur, 1981) or 2.10(7) Å (Serezhkin *et al.*, 2003), towards the value of pure Al compounds, 1.909 Å (Baur, 1981). The mean T–O bond length in the $(As,P)O_4$ tetrahedron, 1.656 Å, is between those of pure arsenates and phosphates (see above), and reflects the partial substitution of P for As. As in the four variscite-type compounds, the O ligands O1–4 in bonacinaite are all somewhat underbonded and, accordingly, acceptors of hydrogen bonds (Table 7). The latter are of medium

https://doi.org/10.1180/mgm.2020.57 Published online by Cambridge University Press

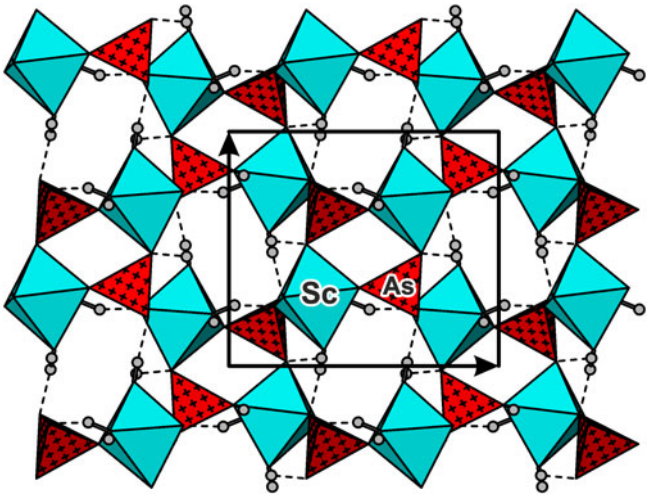

Fig. 3. Polyhedral representation of the framework crystal structure of metavariscite-type bonacinaite, $(Sc,Al)(As,P)O_4{\cdot}2H_2O$, in a view along [100]. Hydrogen bonds are shown with dashed lines. The unit cell is outlined. Note the channels parallel to [100], which are relatively large by comparison to the denser variscite-type structures (Fig. 2).

strength and range between 2.644(4) and 2.813(4) Å (Table 7); two further, long hydrogen bonds to O3 and O1 at 3.258(4) and 3.152(4) Å, respectively, show that the bonds involving Ow1 and H11, and Ow2 and H22, are bifurcated.

Structure comparison

For a quantitative comparison of the isotypic crystal structures within the variscite and metavariscite groups, respectively, the program *COMPSTRU* (de la Flor *et al.*, 2016) available at the Bilbao Crystallographic Server (Aroyo *et al.*, 2006) was used. The criterion for this comparison is based on a full crystal-structure analysis from single-crystal diffraction data and a reliability factor $R_1 < 0.05$. Except for variscite-type $TlPO_4{\cdot}2H_2O$ and $TlAsO_4{\cdot}2H_2O$ (Schroffenegger *et al.*, 2020), for which diffraction data were recorded at −173°C, all other crystals were measured at room temperature. The effect of the temperature on unit-cell parameters was neglected for the two cases. Due to different treatments of H atoms in the various refinements, e.g. by constrains/restraints regarding O–H bond lengths, our comparisons do not include hydrogen atoms.

Variscite (Kniep *et al.*, 1977) and metavariscite (Kniep and Mootz, 1973), respectively, were chosen as references, to which all other crystal structures in the corresponding groups were compared. For that purpose, literature data were standardised in terms of atom labelling and space-group setting and then were related to the reference structures. In the case of variscite, a cyclic transformation and a shift of the origin was necessary for some cases. In the case of metavariscite, all structures (including metavariscite itself) were transformed into the standard setting of space group type no. 14 ($P2_1/c$).

In Tables 8 and 9, numerical results of the comparisons are given, listing displacements of individual atoms relative to the standard. Also compiled are the degree of lattice distortion (**S**) which is the spontaneous strain, i.e. the sum of the squared eigenvalues of the strain tensor divided by 3, the arithmetic mean (d_{av}) of the distances and the measure of similarity (Δ) (Bergerhoff *et al.*, 1999). The latter is a function of the differences in atomic positions (weighted by the multiplicities of the sites) and the ratios of the corresponding unit-cell parameters of the structures (de la Flor *et al.*, 2016).

In terms of atomic displacements, there is no clear trend recognisable for the variscite group, which may reflect the flexibility of the shared atomic arrangement. In the majority of cases (ten out of thirteen), atom O3 (which is one of the ligands linking $MO_4(H_2O)_2$ octahedra to TO_4 tetrahedra) shows the highest displacement in the crystal structure. The lowest displacements are shown by the O atom that belongs to water molecule Ow2 (six cases), the metal atom M (five cases) and the T atom in the TO_4 tetrahedron (two cases). On the other hand, in the metavariscite group the trend regarding maximum and minimum atomic displacements is somewhat clearer: in four out of five cases, the maximum value is associated with the O atom of the water molecule Ow2 (Ow1 has the second highest values in all cases), and the minimum value pertains to the tetrahedrally coordinated T atoms. Thus, the TO_4 groups behave, not surprisingly, as a rigid building unit.

The most informative parameter from the comparisons is the measure of similarity (Δ). The smaller the number of Δ, the higher is the similarity of the two compared structures, with Δ = 0.114 for $CdSeO_4{\cdot}2H_2O$ being the maximum value for all structures. For both variscite and metavariscite groups, Δ appears not to depend on the variation of M1 and X1 or their formal charges in the dimorphic $MXO_4{\cdot}2H_2O$ compounds, but clearly on the crystal volume. Within a roughly linear correlation, Δ increases with increasing volume (Fig. 4).

From the viewpoint of topology, both variscite and metavariscite are based upon four-connected 3D frameworks based upon simple hexagonal 2D nets. Note that, despite the fact that both variscite and metavariscite are based upon octahedral–tetrahedral frameworks, only four vertices of each AlO_6 octahedron are bridging, whereas the two remaining ones are occupied by H_2O molecules and do not participate in the intraframework linkage. Wells (1954) and Smith (1977) derived a number of 3D nets based upon hexagonal nets linked in the direction perpendicular to the net plane. Figure 5a and c shows the hexagonal net in the metavariscite and variscite frameworks, respectively, with black and white nodes pointed upward and downward, respectively. According to Smith (1977), two adjacent nodes in a hexagon can have the additional linkages pointing in either the same (**S**) or changed (**C**) direction, respectively. Thus, each edge of the net is associated with either the **S** or **C** symbol. The metavariscite 3D net is based upon the 2D net with the cyclic symbol **SCCSCC** (Fig. 5*a*), whereas that in variscite has the symbol **SCSCCC** (Fig. 5*c*). The linkage of the hexagonal 2D nets in both metavariscite and variscite results in the formation of four-membered rings oriented perpendicular to the 2D nets. The idealised topologies of the metavariscite and variscite frameworks are shown in Fig. 5*b* and *d*, respectively.

The metavariscite topology corresponds to the **BCT** type of zeolite topologies, which was observed in the framework alkali silicates with Si^{4+} replaced by Mg^{2+}, Zn^{2+} or Fe^{2+} (type material: Dollase and Ross, 1993) and in svyatoslavite, a metastable polymorph of anorthite, $CaAl_2Si_2O_8$ (Chesnokov *et al.*, 1989; Krivovichev *et al.*, 2012). The ideal symmetry of the BCT framework is described by the tetragonal space group $I4/mmm$. In metavariscite, the symmetry is reduced to $P2_1/n$, which is a subgroup of $I4/mmm$. The symmetry reduction can be viewed as consisting of two steps: the $I4/mmm \rightarrow P4_2/mnm$ transition due to the Al–P ordering of the framework nodes and the $P4_2/mnm \rightarrow P2_1/n$ transition due to the framework distortion. The topology is based upon four-membered rings of tetrahedra stacked in

https://doi.org/10.1180/mgm.2020.57 Published online by Cambridge University Press

Table 8. Numerical details from the comparisons of the crystal structure of variscite ($AlPO_4·2H_2O$) with isotypic structures[1)] of the variscite group using the *COMPSTRU* program (de la Flor *et al.*, 2016).

$AlPO_4·2H_2O$	$FePO_4·2H_2O$ (Taxer and Bartl, 2004)	$GaPO_4·2H_2O$ (Loiseau, 1998)	$InPO_4·2H_2O$ (Xu *et al.*, 1995)	$TlPO_4·2H_2O$ (this work)	$AlAsO_4·2H_2O$ (Harrison, 2000)	$CrAsO_4·2H_2O$ (this work)
Transformation matrix (P; p) [2)]	**c, a, b;** 0,0,½	**a, b, c;** 0,0,0	**c, a, b;** ½,½,½	**a, b, c;** 0,0,0	**c, a, b;** 0,0,0	**a, b c,;** 0,0,0
Atom, atomic displacement |u| /Å						
Al1/*M*1	0.0379	0.0265	0.0515	0.1198	0.1380	0.1275
P1/*X*1	0.0174	0.0310	0.0655	0.1444	0.0949	0.1072
O1	0.0616	0.0786	0.1762	0.3095	0.1997	0.2337
O2	0.0667	0.0767	0.1997	0.3109	0.1189	0.1653
O3	0.0673	0.0920	0.2112	0.3920	0.1928	0.2587
O4	0.0534	0.0608	0.1440	0.1983	0.2138	0.2221
OW1	0.0792	0.0762	0.1799	0.2999	0.1715	0.1666
OW2	0.0664	0.0460	0.1325	0.1933	0.1534	0.0990
Degree of lattice distortion (S)	0.0141	0.0061	0.0260	0.0292	0.0151	0.0202
Arithmetic mean (d_{av})	0.0562	0.0610	0.1451	0.2460	0.1604	0.1725
Measure of similarity (Δ)	0.024	0.010	0.034	0.054	0.033	0.032

$AlPO_4·2H_2O$	$FeAsO_4·2H_2O$ (Xu *et al.*, 2007)	$GaAsO_4·2H_2O$ (Dick, 1997)	$InAsO_4·2H_2O$ (Chen *et al.*, 2002)	$TlAsO_4·2H_2O$ (Schroffenegger *et al.*, 2020)	$MnSeO_4·2H_2O$ (this work, crystal 1)
Transformation matrix (P; p) [2)]	**c, a, b;** 0,½,½	**a, b, c;** 0,0,0	**c, a, b;** 0,0,0	**a, b, c;** 0,0,0	**a, b, c;** 0,0,0
Atom, atomic displacement |u| /Å					
Al/M	0.1686	0.1480	0.1631	0.1860	0.0458
P/T	0.1182	0.1215	0.1669	0.2156	0.0989
O1	0.2167	0.2375	0.2902	0.3789	0.1967
O2	0.1467	0.1546	0.2570	0.3451	0.1722
O3	0.2520	0.2749	0.3812	0.4985	0.2532
O4	0.2164	0.2301	0.2515	0.2838	0.1425
Ow1	0.1613	0.1768	0.2406	0.3286	0.2481
Ow2	0.0916	0.1129	0.0760	0.1587	0.0947
Degree of lattice distortion (S)	0.0258	0.0186	0.0353	0.0389	0.0413
Arithmetic mean (d_{av})	0.1714	0.1820	0.2283	0.2994	0.1565
Measure of similarity (Δ)	0.040	0.029	0.039	0.071	0.071

$AlPO_4·2H_2O$	$CdSeO_4·2H_2O$ (this work)	$ZnSeO_4·2H_2O$ (Krivovichev, 2007)
Transformation matrix (P; p)[1)]	**a, b, c;** 0,0,0	**c, a, b;** 0,0,½
Atom, atomic displacement |u|/Å		
Al/M	0.0615	0.0664
P/T	0.1269	0.0901
O1	0.2452	0.2006
O2	0.2500	0.1474
O3	0.3153	0.2492
O4	0.1803	0.1636
Ow1	0.3519	0.2299
Ow2	0.2071	0.0640
Degree of lattice distortion (S)	0.0484	0.0305
Arithmetic mean (d_{av})	0.2173	0.1514
Measure of similarity (Δ)	0.114	0.039

[1)]Atom labelling refers to the refinements in this study and corresponds to that originally given for variscite (Kniep *et al.*, 1977).
[2)]P is the transformation and p is the shift of origin used for standardisation of crystal data relative to variscite.

columns along the *c* axis and interlinked with similar rings in the adjacent columns (Fig. 5*b*).

The variscite topology was first recognised by Smith (1977) as the topology of the gallate framework in monoclinic $CaGa_2O_4$ (Deiseroth and Müller-Buschbaum, 1973). Its ideal symmetry is described by the space group *Cmca*, which, due to the Al–P ordering, is reduced to its subgroup *Pbca* as observed in variscite. Whereas four-membered rings in the metavariscite topology are parallel to each other (Fig. 5*b*), they are inclined relative to each other in the variscite topology (Fig. 5*d*).

Relative stabilities of the two structure types

From our survey of the literature and the study of the title compounds and minerals, it appears not fully clear whether one of the two atomic arrangements can be considered thermodynamically more stable at ambient temperature, and how large the influence of kinetics and other parameters (e.g. pH) is. From hydrothermal syntheses of metavariscite and variscite, Sergeeva (2016) concluded that metavariscite is the high-temperature dimorph and variscite the low-temperature one; both were found to coexist at a temperature of ~63°C. In a detailed study on natural strengite and phosphosiderite, Wilk (1959) observed that phosphosiderite shows a reversible transformation at 95°C, but the nature of the high-temperature phase was not identified (the high-temperature Guinier powder pattern does not resemble that of strengite); this transformation may be related to a partial dehydration. A mixture of synthetic strengite and its dimorph phosphosiderite from hydrolysis of $Fe(H_2PO_4)_3·H_2O$ at pH 2.8 was obtained by Eshchenko *et al.* (1973). Strengite and phosphosiderite, as well

https://doi.org/10.1180/mgm.2020.57 Published online by Cambridge University Press

Table 9. Numerical details from the comparisons of the crystal structure of metavariscite-type $AlPO_4·2H_2O$ (Kniep and Mootz, 1973) with isotypic structures[1)] of the metavariscite group using the *COMPSTRU* program (de la Flor *et al.*, 2016).

$AlPO_4·2H_2O$	$FePO_4·2H_2O$ (Taxer and Bartl, 2004)	$InPO_4·2H_2O$ (Sugiyama *et al.*, 1999)	$VPO_4·2H_2O$ (Schindler *et al.*, 1995)	$ScPO_4·2H_2O$ (Yang *et al.*, 2007)	$ScAsO_4·2H_2O$ (this work)
Transformation matrix (P; p)	**a, b, c;** 0,0,0	**a, b, c;** 0,0,0	**a, b, c;** 0,0,0	**a, b, c;** 0,0,0	**a, b, c;** 0,0,0
Atom, atomic displacement |u| /Å					
Al/M	0.0328	0.0662	0.0446	0.1156	0.0904
P/T	0.0312	0.0329	0.0198	0.0773	0.0598
O1	0.0506	0.1850	0.1070	0.2025	0.1946
O2	0.0526	0.1579	0.0858	0.1204	0.1715
O3	0.0843	0.1975	0.1109	0.1852	0.1630
O4	0.0732	0.1709	0.0723	0.1905	0.0833
Ow1	0.0653	0.2986	0.1837	0.2650	0.3763
Ow2	0.0762	0.2535	0.1463	0.2321	0.2697
Degree of lattice distortion (S)	0.0171	0.0320	0.0160	0.0311	0.0404
Arithmetic mean (d_{av})	0.0583	0.1703	0.0963	0.1736	0.1761
Measure of similarity (Δ)	0.017	0.058	0.029	0.054	0.058

[1)]Atom labelling refers to the refinements in this study and corresponds to that originally given for metavariscite (Kniep and Mootz, 1973).

as variscite and metavariscite, can also coexist in natural assemblages (e.g. phosphate pegmatites), suggesting very small differences in their Gibbs energy of formation. To our knowledge, only values for strengite and variscite have been determined (Robie *et al.*, 1979, and Woods and Garrels, 1987, respectively), but none for phosphosiderite or metavariscite. The X-ray density values of dimorphic pairs are distinctly different: for strengite, $D_x = 2.85$ mg m^{-3}, while for phosphosiderite, $D_x = 2.72$ mg m^{-3} (Taxer and Bartl, 2004); for variscite, $D_x = 2.59$ mg m^{-3} (Kniep *et al.*, 1977), whereas metavariscite has $D_x = 2.535$ mg m^{-3} (Kniep and Mootz, 1973). This clearly demonstrates that the orthorhombic modification in the phosphate subgroups is denser and therefore can be considered more stable. The case is less clear-cut when synthetic $InPO_4·2H_2O$ is considered: The orthorhombic dimorph has $D_x = 3.294$ mg m^{-3} (Tang *et al.*, 2002), while the monoclinic dimorph has $D_x = 3.300$ (Sugiyama *et al.*, 1999).

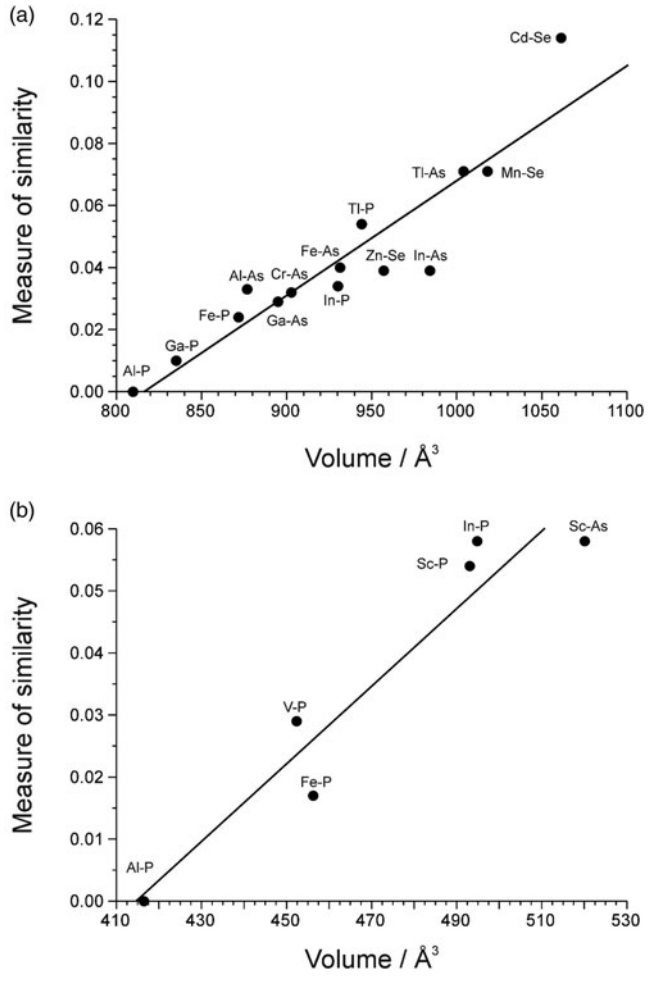

Fig. 4. Dependence of the measure of similarity on the crystal volume for the variscite group (*a*) and the metavariscite group (*b*).

The influence of pH also plays a role: in the case of synthetic dimorphic $InPO_4·2H_2O$ (Sugiyama *et al.*, 1999), crystallisation of the variscite-type dimorph was favoured when mixtures with a higher H_3PO_4 content were used. The resulting lower pH may lead to a change in speciation in the hydrothermal fluid, and to the formation of polynuclear complexes that may then template specific crystalline solids. This observation suggests that (metastable?) metavariscite-type $InAsO_4·2H_2O$ might be prepared under certain pH conditions and/or at elevated temperatures.

It is worth noting that Strunz and von Sztrokay (1939) stated that the existence of a monoclinic, metavariscite-type "clinoscorodite" in nature is probable. However, such a dimorph was never confirmed in the numerous studies on the preparation and stability of scorodite, although it might crystallise from high (er)-temperature hydrothermal solutions if strongly stabilised in some way.

Topological and structural complexity and stability

The relative complexity of the structures and topologies of variscite and metavariscite can be analysed using the information complexity measures proposed in Krivovichev (2012, 2013*a*,*b*, 2014). Within this approach, the crystal-structure complexity is numerically estimated as the amounts of structural Shannon information per atom ($^{str}I_G$) and per unit cell ($^{str}I_{G,total}$), calculated according to the following equations:

$$^{str}I_G = -\sum_{i=1}^{k} p_i \log_2 p_i \text{ (bits/atom)} \quad (1)$$

https://doi.org/10.1180/mgm.2020.57 Published online by Cambridge University Press

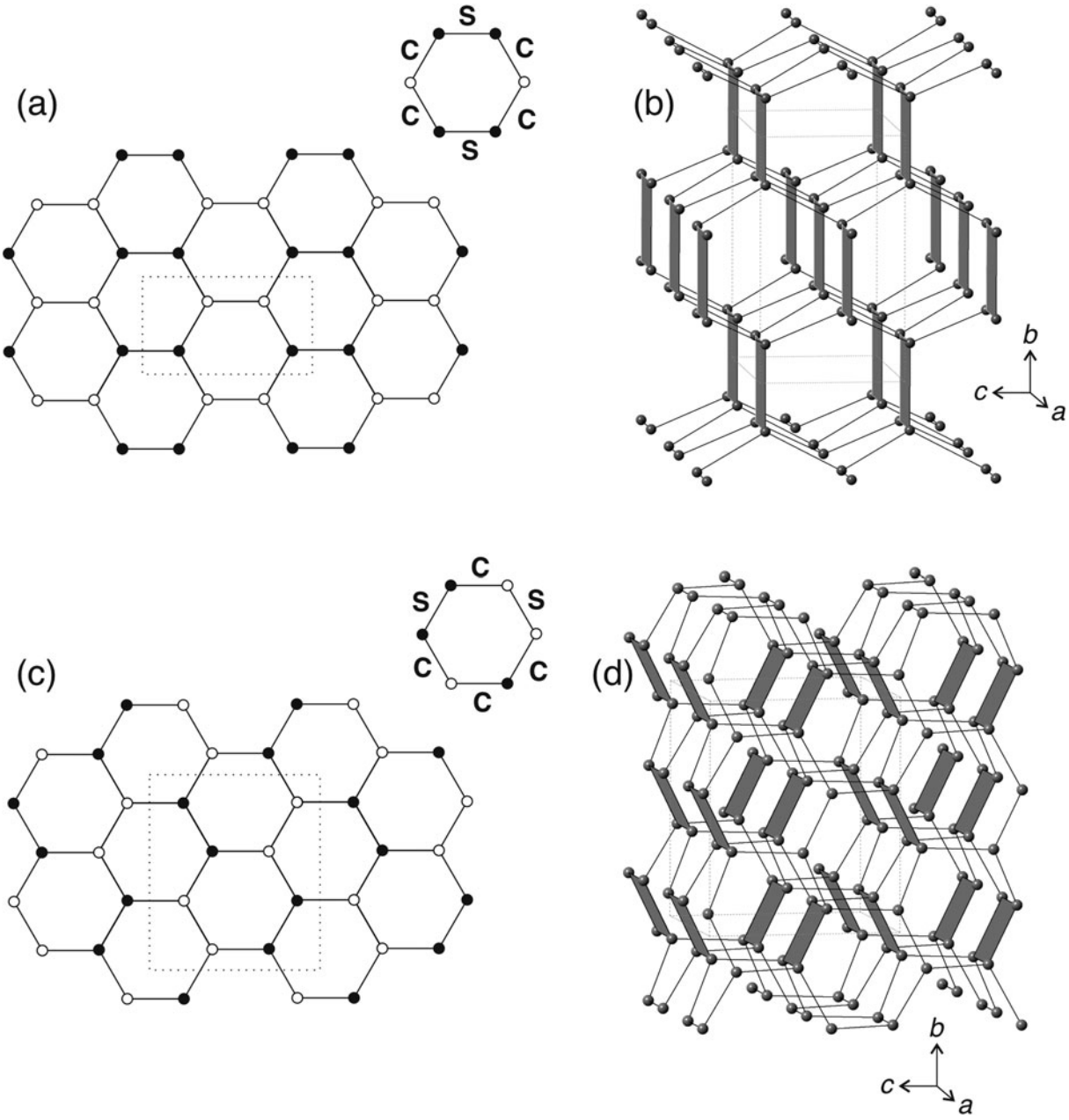

Fig. 5. Idealised topologies of frameworks in metavariscite (*a*, *b*) and variscite (*c*, *d*). The black and white vertices in the simple hexagonal nets in (*a*, *c*) correspond to the up and down linkages, respectively. The grey squares in (*b*, *d*) highlight the location of the four-membered rings. See text for details.

$$^{str}I_{G,total} = -vI_G = -v \sum_{i=1}^{k} p_i \log_2 p_i \text{ (bits/cell)} \quad (2)$$

where k is the number of different crystallographic orbits in the structure and p_i is the random choice probability for an atom from the ith crystallographic orbit, that is:

$$p_i = m_i/v \quad (3)$$

where m_i is a multiplicity of a crystallographic orbit (i.e. the number of atoms of a specific Wyckoff site in the reduced unit cell), and v is the total number of atoms in the reduced unit cell.

Table 10. Information-based complexity parameters for variscite and metavariscite (v in atoms per cell, I_G in bit per atom and $I_{G,total}$ in bits per cell).

	Framework topological complexity				Total structural complexity			
Mineral	Sp. gr.	v	I_G	$I_{G,total}$	Sp. gr.	v	I_G	$I_{G,total}$
Metavariscite	*I*4/*mmm*	12	1.585	19.020	$P2_1/n$	48	3.585	172.078
Variscite	*Cmca*	12	2.252	27.020	*Pbca*	96	3.585	344.156

Sp. gr. – space group.

The topological complexity is calculated by taking into account the complexity of the idealised framework topology, where each T atom (T = Al or P) is associated with a node, and each edge is

https://doi.org/10.1180/mgm.2020.57 Published online by Cambridge University Press

Table 11. List of selected phases of the variscite and metavariscite groups as potential electrode materials for Li ion batteries.

Space group	Initial material (mineral name)	Final material	Redox couple	Theoretical capacity (mAh/g)	Experimental capacity (mAh/g)	Average potential (V *vs.* Li)
Pbca	$FePO_4·2H_2O$ (strengite)	$LiFePO_4·2H_2O$	Fe^{3+}/Fe^{2+}	143.4	~140[1)]	~3.0[1)]
Pbca	$FeAsO_4·2H_2O$ (scorodite)	$LiFeAsO_4·2H_2O$	Fe^{3+}/Fe^{2+}	116.1	n.d.	~3.0[2)]
$P2_1/n$	$FePO_4·2H_2O$ (phosphosiderite)	$LiFePO_4·2H_2O$	Fe^{3+}/Fe^{2+}	143.4	~120[1)]	~3.0[1)]
$P2_1/n$	$VPO_4·2H_2O$	$LiVPO_4·2H_2O$	V^{3+}/V^{2+}	147.3	n.d.	< 2.0[2)]

[1)]Experimental values from Delacourt *et al.* (2009)
[2)]Expected values, see details in text.
n.d. – not determined.

associated with the O atom in the middle of the T–T link (Krivovichev, 2013*b*).

The topological and structural complexity parameters for variscite and metavariscite are given in Table 10. It can be seen that variscite is both structurally and topologically more complex than metavariscite. This kind of complexity relations is observed for stable and metastable polymorphs that form in an Ostwald sequence of phases in inorganic systems. According to the Goldsmith's simplexity principle (Goldsmith, 1953), metastable kinetically stabilised phases in the Ostwald cascades are usually structurally simpler than their thermodynamically stable polymorphs. Krivovichev (2013*a*) confirmed the validity of this principle using information-based complexity measures, and several other examples have been accumulated recently (Cempírek *et al.*, 2016; Zaitsev *et al.*, 2017; Krivovichev *et al.*, 2017; Plášil *et al.*, 2017; Plášil, 2018; Majzlan *et al.*, 2018; Huskić *et al.*, 2019; Majzlan, 2020). Thus, metavariscite and phosphosiderite can be considered as metastable phases, in contrast to their stable counterparts, variscite and strengite, respectively. This hypothesis is in agreement with the differences in the physical densities (see above): according to the Ostwald–Volmer rule, the polymorphs with the lowest density in Ostwald sequences are formed first (Bach *et al.*, 2013). The difference in complexity between variscite and metavariscite is also in agreement with the identification of the two phases as low- and high-temperature polymorphs, respectively (Sergeeva, 2016), as the empirical rule states that the high-temperature phase is usually less complex than the low-temperature phase (Krivovichev, 2013*a*).

Compounds of the variscite and metavariscite groups as potential electrode materials

Both $FePO_4·2H_2O$ polymorphs, orthorhombic strengite and monoclinic phosphosiderite, have been the subject of several studies focused on evaluation of their electrochemical properties (Hong *et al.*, 2002; Masquelier *et al.*, 2002; Song *et al.*, 2002*a*; Delacourt *et al.*, 2009). In particular, these compounds, composed of abundant and low-cost elements, look attractive as they provide 3D frameworks suitable for small-sized ion intercalation. Moreover, the presence of transition metal cations in the structure of strengite and phosphosiderite suggests that it would operate on the Fe^{3+}/Fe^{2+} redox couple and might be used as an electrode material in a rechargeable Li ion battery with a promising theoretical specific capacity value of 143.4 mAh/g. Indeed, the crystalline and amorphous $FePO_4·2H_2O$ phases were promptly patented by Masquelier *et al.* (2003), and after a while Delacourt *et al.* (2009) revealed a decent electrochemical behaviour of both variscite- and metavariscite-type crystalline phases with a good capacity retention delivering reversible capacities of ~140 and 120 mAh/g, respectively, at an average potential of ~3 V *vs.* Li^+/Li. Delacourt *et al.* (2009) also observed a beneficial role of constitutional water molecules promoting fast ionic conduction.

The better performance of variscite-type strengite agrees well with our findings about the structural stability of the polymorphs: the denser and more complex variscite-type framework provides appropriate stability essential for extensive electrochemical (de) intercalation of Li into its crystal structure.

In view of the foregoing, $VPO_4·2H_2O$ (Schindler *et al.*, 1995) would be also of interest to investigate the formation of a theoretical $Li_xVPO_4·2H_2O$ composition (theoretical specific capacity of 147.3 mAh/g) by electrochemical lithiation. It is important to note, however, that the reduction mechanism of V^{3+} to V^{2+} generally occurs through lithium insertion at a quite low potential of <2 V *vs.* Li^+/Li (Masquelier and Croguennec, 2013). Hence, a positive effect of higher theoretical capacity of the vanadium-based phase can be diminished by low operating voltages in practical tests.

In this regard, scorodite, $FeAsO_4·2H_2O$, is worthy of the attention as well as the inductive effect (Padhi *et al.*, 1997) of As^{5+} cations on the Fe^{3+}/Fe^{2+} couple is similar to that of P^{5+} due to close electronegativity values of As and P (Allen, 1989). Thus, the Fe^{3+}/Fe^{2+} redox process would probably occur at a similar potential value of ~3 V *vs.* Li^+/Li. This phase exhibits a moderate theoretical capacity (116 mAh/g), which also promotes further electrochemical tests.

The summarising list of selected candidates for the role of electrode materials in Li ion batteries is given in Table 11.

Supplementary material. To view supplementary material for this article, please visit https://doi.org/10.1180/mgm.2020.57

Acknowledgements. Part of this work was done while the first author was financially supported by the Austrian Science Foundation (FWF). S.V.K was supported in this work by the Russian Science Foundation (grant 19-17-00038). V.K. would like to thank Olivier Mentré, Marie Colmont and Almaz Aliev from the UCCS laboratory (University of Lille 1) for providing laboratory equipment for the synthesis of $MnSeO_4·2H_2O$ (method 2). The article was improved by constructive reviews by Juraj Majzlan and two anonymous reviewers and editorial assistance by Principal Editor Stuart Mills.

References

Allen L.C. (1989) Electronegativity is the average one-electron energy of the valence-shell electrons in ground-state free atoms. *Journal of the American Chemical Society*, **111**, 9003–9014.

Arlidge E.Z., Farmer V.C., Mitchell B.D. and Mitchell W.A. (1963) Infrared, x-ray, and thermal analyses of some aluminum and ferric phosphates. *Journal of Applied Chemistry (London)*, **13**, 17–27.

Aroyo M.I., Perez-Mato J.M., Capillas C., Kroumova E., Ivantchev S., Madariaga G., Kirov A. and Wondratschek H. (2006) Bilbao Crystallographic Server I: Databases and crystallographic computing programs. *Zeitschrift für Kristallographie*, **221**, 15–27.

Bach A., Fischer D. and Jansen M. (2013) Metastable phase formation of indium monochloride from an amorphous feedstock. *Zeitschrift für Anorganische und Allgemeine Chemie*, **639**, 465–467.

Barresi A.A., Kolitsch U., Ciriotti M.E., Ambrino P., Bracco R. and Bonacina E. (2005) La miniera di manganese di Varenche (Aosta, Italia nord-occidentale): ardennite, arseniopleite, manganberzeliite, pirofanite, sarkinite, sursassite, thortveitite, nuovo As-analogo della metavariscite e altre specie minerali. *Micro*, **2005** (2), 81–122 [in Italian].

Baur W.H. (1981) Interatomic distance predictions for computer simulation of crystal structures. Pp. 31–52 in: *Structure and Bonding in Crystals II* (M. O'Keeffe and A. Navrotsky, editors). Academic Press, New York.

Belsky A., Hellenbrandt M., Karen V.L. and Luksch P. (2002) New developments in the Inorganic Crystal Structure Database (ICSD): accessibility in support of materials research and design. *Acta Crystallographica*, **B58**, 364–369.

Bennett J.M., Dytrych W.J., Pluth J.J., Richardson J.W., Jr. and Smith J.V. (1986) Structural features of aluminophosphate materials with aluminum/phosphorus = 1. *Zeolites*, **6**, 349–360.

Bergerhoff G., Berndt M., Brandenburg K. and Degen T. (1999) Concerning inorganic crystal structure types. *Acta Crystallographica*, **B55**, 147–156.

Bolanz R.M., Wierzbicka-Wieczorek M., Giester G., Göttlicher J. and Steininger R. (2016) Structural incorporation of As^{5+} into phosphosiderite by a strengite/scorodite-like arrangement. *ChemistrySELECT*, **1**, 4152–4160.

Borensztajn J. (1965) Crystal structures of metavariscite and metastrengite. *Comptes Rendus de l'Académie des Sciences*, **261**, 376–378 [in French].

Borensztajn J. (1966) Crystalline structure of metavariscite and metastrengite. *Bulletin de la Société Française de Minéralogie et de Cristallographie*, **89**, 428–438 [in French].

Botelho N.F., Roger G., D'Yvoire F., Moëlo Y. and Volfinger M. (1994) Yanomamite, $InAsO_4{\cdot}2H_2O$, a new indium mineral from topaz-bearing greisen in the Goiás tin province, Brazil. *European Journal of Mineralogy*, **6**, 245–254.

Brown I.D. (1996) *VALENCE*: a program for calculating bond-valences. *Journal of Applied Crystallography*, **29**, 479–480.

Bruker AXS (1997) *SHELXTL, Version 5.1*. Bruker AXS, Inc., Madison, WI 53719, USA.

Bruker AXS (1998*a*) *SMART, Version 5.0*. Bruker AXS, Inc., Madison, WI 53719, USA.

Bruker AXS (1998*b*) *SAINT, Version 5.0*. Bruker AXS, Inc., Madison, WI 53719, USA.

Bull I., Young V., Teat S.J., Peng L., Grey C.P. and Parise J.B. (2003) Hydrothermal Synthesis and structural characterization of four scandium phosphate frameworks. *Chemistry of Materials*, **15**, 3818–3825.

Cámara F., Ciriotti M.E., Kolitsch U., Vignola P., Hatert F., Bittarello E., Bracco R. and Bortolozzi G.M. (2018) Bonacinaite, IMA 2018-056. CNMNC Newsletter No. 45, October 2018, pages 1228–1229; *Mineralogical Magazine*, **82**, 1225–1232.

Carron M.K., Mrose M.E. and Murata K.J. (1958) Relation of ionic radius to structures of rare-earth phosphates, arsenates, and vanadates. *American Mineralogist*, **43**, 985–989.

Cempírek J., Grew E.S., Kampf A.R., Ma C., Novák M., Gadas P., Škoda R., Vašinová-Galiová M., Pezzotta F., Groat L.A. and Krivovichev S.V. (2016) Vránaite, ideally $Al_{16}B_4Si_4O_{38}$, a new mineral related to boralsilite, $Al_{16}B_6Si_2O_{37}$, from the Manjaka pegmatite, Sahatany Valley, Madagascar. *American Mineralogist*, **101**, 2108–2117.

Chen Z.-X., Weng L.-H., Zhou Y.-M., Zhang H.-Y. and Zhao D.-Y. (2002) Synthesis and structure of a new three-dimensional microporous indium arsenate. *Huaxue Xuebao*, **60**, 305–309 [in Chinese].

Chesnokov B.V., Lotova E.V., Pavlyuchenko V.S., Nigmatulina E.N., Usova L.V., Bushmakin A.R. and Nishanbaev T.P. (1989) Svyatoslavite, $CaAl_2Si_2O_8$ (orthorhombic), a new mineral. *Zapiski Vsesoyuznogo Mineralogicheskogo Obshchestva*, **118**, 111–114 [in Russian].

de la Flor G., Orobengoa D., Tasci E., Perez-Mato J.M. and Aroyo M.I. (2016) Comparison of structures applying the tools available at the Bilbao Crystallographic Server. *Journal of Applied Crystallography*, **49**, 653–664.

Deiseroth H.J. and Müller-Buschbaum H. (1973) Über Erdalkalimetalloxogallate. III. Untersuchung des Aufbaus von $CaGa_2O_4$. *Zeitschrift für Anorganische und Allgemeine Chemie*, **396**, 157–164 [in German].

Delacourt C., Poizot P., Bonnin D. and Masquelier C. (2009) Lithium-insertion mechanism in crystalline and amorphous $FePO_4{\cdot}nH_2O$. *Journal of the Electrochemical Society*, **156**, A595–A605.

Demassieux N. (1945) Dehydration of the double selenate of nickel and potassium. *Comptes rendus*, **221**, 557–558 [in French].

Dick S. (1997) Die Struktur von $GaAsO_4{\cdot}2H_2O$: Ein neues Mitglied der Variscit-Familie. *Zeitschrift für Naturforschung*, **B52**, 1337–1340 [in German].

Dollase W.A. and Ross C.R. (1993) Crystal structures of body-centered tetragonal tectosilicates: $K_{1.14}Mg_{0.57}Si_{1.43}O_4$, $K_{1.10}Zn_{0.55}Si_{1.45}O_4$, and $K_{1.11}Fe_{1.11}Si_{0.89}O_4$. *American Mineralogist*, **78**, 627–632.

Dowty E. (2011) *ATOMS V6.4.0 for Atomic-Structure Display*. Shape Software, 521 Hidden Valley Road, Kingsport, TN 37663 USA.

Elton N.J. (1996) Variscite and metavariscite from Gunheath china clay pit, St Austell, Cornwall. *Mineralogical Magazine*, **60**, 671–672.

Eshchenko L.S., Shchegrov L.N., Pechkovskii V.V. and Ustimovich A.B. (1973) Crystal hydrates of trisubstituted iron(III) orthophosphate. *Zhurnal Neorganicheskoi Khimii*, **18**, 909–914 [in Russian].

Euler H., Meents A., Barbier B. and Kirfel A. (2003) Crystal structure of tetraaquamanganese(II) selenate monohydrate, $Mn(H_2O)_4SeO_4{\cdot}H_2O$. *Zeitschrift für Kristallographie – New Crystal Structures*, **218**, 9–10.

Fanfani L. and Zanazzi P.F. (1966) Crystalline structure of metastrengite. *Atti dell'Accademia Nazionale dei Lincei. Rendiconti. Classe di scienze fisiche, matematiche e naturali*, **40**, 880–889 [in Italian].

Fayos J. and Salvador-Salvador P. (1971) A systematic approximate method for the determination of structure factors from a powder diffractogram and its application to the solution of the structure of metavariscite. *Journal of Applied Crystallography*, **4**, 159–163.

Gagné O.C. and Hawthorne F.C. (2015) Comprehensive derivation of bond-valence parameters for ion pairs involving oxygen. *Acta Crystallographica*, **B71**, 562–578.

Gagné O.C. and Hawthorne F.C. (2018) Bond-length distributions for ions bonded to oxygen: metalloids and post-transition metals. *Acta Crystallographica*, **B74**, 63–78.

Goldsmith J.R. (1953) A "simplexity principle" and its relation to "ease" of crystallization. *Journal of Geology*, **61**, 439–451.

Harrison W.T.A. (2000) Synthetic mansfieldite, $AlAsO_4{\cdot}2H_2O$. *Acta Crystallographica*, **C56**, e421.

Hawthorne F.C. (1976) The hydrogen positions in scorodite. *Acta Crystallographica*, **B32**, 2891–2892.

Hong Y.-S., Ryu K.S., Park Y.J., Kim M.G., Lee J.M. and Chang S.H. (2002) Amorphous $FePO_4$ as 3 V cathode material for lithium secondary batteries. *Journal of Materials Chemistry*, **12**, 1870–1874.

Huminicki D.M.C. and Hawthorne F.C. (2002) The crystal chemistry of the phosphate minerals. Pp 123–253 in: *Phosphates* (M.L. Kohn, J. Rakovan and J.M. Hughes, editors). Reviews in Mineralogy and Geochemistry, **vol. 48**. Mineralogical Society of America and the Geochemical Society, Washington DC.

Huskić I., Novendra N., Lim D.-W., Topić F., Titi H.M., Pekov I.V., Krivovichev S.V., Navrotsky A., Kitagawa H. and Friščić T. (2019) Functionality in metal-organic framework minerals: proton conductivity, stability and potential for polymorphism. *Chemical Science*, **10**, 4923–4929.

Ilyushin G.D. and Blatov V.A. (2017) Symmetry and topology code of the cluster self-assembly of framework MT structures of alumophosphates $AlPO_4(H_2O)_2$ (metavariscite and variscite) and $Al_2(PO_4)_2(H_2O)_3$ (APC). *Crystallography Reports*, **62**, 174–184.

Ivanov-Emin B.N., Korotaeva L.G., Moskalenko V.I. and Ezhov A.I. (1971) Scandium arsenates. *Zhurnal Neorganicheskoi Khimii*, **16**, 2925–2928 [in Russian].

Kitahama K., Kiriyama R. and Baba Y. (1975) Refinement of the crystal structure of scorodite. *Acta Crystallographica*, **B31**, 322–324.

Kleber W. and Weiner K.L. (1958) Comparative crystallographic studies of the orthorhombic phosphates and arsenates of the type $Y(zO_4){\cdot}2H_2O$. *Neues Jahrbuch für Mineralogie, Abhandlungen*, **90**, 253–284.

Klein A. (1940) The selenates of the metals of the magnesium series. *Annali di Chimica Applicata*, **14**, 263–317.

Kniep R. and Mootz D. (1973) Metavariscite – a redetermination of its crystal structure. *Acta Crystallographica*, **B29**, 2292–2294.

https://doi.org/10.1180/mgm.2020.57 Published online by Cambridge University Press

Kniep R., Mootz D. and Vegas A. (1977) Variscite. *Acta Crystallographica*, **B33**, 263–265.

Kokkoros P. (1939) Comparative x-ray studies of arsenates and selenates. *Neues Jahrbuch für Mineralogie und Geologie (Ref. I)*, **1939**, 252–253.

Koleva V. and Stoilova D. (1997) Thermal dehydration of cobalt selenate hydrates. *Thermochimica Acta*, **296**, 31–36.

Koleva V. and Stoilova D. (1999) DTA, DSC and X-ray studies on copper and manganese selenate hydrates. *Thermochimica Acta*, **342**, 89–95.

Komissarova L.N., Pushkina G.Ya. and Khrameeva N.P. (1971) Preparation and some properties of scandium arsenate dihydrate. *Zhurnal Neorganicheskoi Khimii*, **16**, 1538–1541 [in Russian].

Komissarova L.N., Pushkina G.Ya., Khrameeva N.P. and Teterin E.G. (1973) Scandium arsenates. *Zhurnal Neorganicheskoi Khimii*, **18**, 2316–2323 [in Russian].

Kovrugin V.M., Aliev A., Colmont M., Mentré O. and Krivovichev S.V. (2016) Synthesis and crystal structure of $Mn(SeO_4)\cdot 2H_2O$, a new member of the variscite family of compounds. *EMC2016, 2nd European Mineralogical Conference, 11-15 September 2016, Rimini, Italy*, abstract pp. 16–23.

Krivovichev S.V. (2007) Crystal chemistry of selenates with mineral-like structures. IV. Crystal structure of $Zn(SeO_4)(H_2O)_2$, a new compound with a mixed framework of the variscite type. *Geology of Ore Deposits*, **49**, 542–546.

Krivovichev S.V. (2009) *Structural Crystallography of Inorganic Oxysalts*. International Union of Crystallography Monographs on Crystallography No. 22, 320 pp.

Krivovichev S.V. (2012) Topological complexity of crystal structures: quantitative approach. *Acta Crystallographica*, **A68**, 393–398.

Krivovichev S.V. (2013a) Structural complexity of minerals: information storage and processing in the mineral world. *Mineralogical Magazine*, **77**, 275–326.

Krivovichev S.V. (2013b) Structural and topological complexity of zeolites: An information-theoretic analysis. *Microporous and Mesoporous Materials*, **171**, 223–229.

Krivovichev S.V. (2014) Which inorganic structures are the most complex? *Angewandte Chemie International Edition*, **53**, 654–661.

Krivovichev S.V., Shcherbakova E.P. and Nishanbaev T.P. (2012) The crystal structure of svyatoslavite and evolution of complexity during crystallization of a $CaAl_2Si_2O_8$ melt: A structural automata description. *The Canadian Mineralogist*, **50**, 585–592.

Krivovichev S.V., Hawthorne F.C. and Williams P.A. (2017) Structural complexity and crystallization: the Ostwald sequence of phases in the $Cu_2(OH)_3Cl$ system (botallackite–atacamite–clinoatacamite). *Structural Chemistry*, **28**, 153–159.

Le Berre J.-F., Gauvin R. and Demopoulos G.P. (2007) Synthesis, structure, and stability of gallium arsenate dihydrate, indium arsenate dihydrate, and lanthanum arsenate. *Industrial and Engineering Chemistry Research*, **46**, 7875–7882.

Loiseau T., Paulet C. and Férey G. (1998) Crystal structure determination of the hydrated gallium phosphate $GaPO_4\cdot 2H_2O$, analog of variscite. *Comptes Rendus de l'Académie des Sciences, Série IIc*, **1**, 667–674.

Lukaszewski G.M., Redfern J.P. and Salmon J.E. (1961) Arsenates. Part I. Preparative, phase-diagram, and other preliminary studies of the system chromium(III)-arsenic acid. *Journal of the Chemical Society*, **1961**, 39–43.

Maier A.I., Selivanova N.M. and Terent'eva L.A. (1965) Heat of formation of cobalt selenate. *Zhurnal Fizicheskoi Khimii*, **39**, 1746–1750 [in Russian].

Majzlan J. (2020) Processes of metastable-mineral formation in oxidation zones and mine waste. *Mineralogical Magazine*, **84**, 367–375.

Majzlan J., Dachs E., Benisek A., Plášil J. and Sejkora J. (2018) Thermodynamics, crystal chemistry and structural complexity of the $Fe(SO_4)(OH)(H_2O)_x$ phases: $Fe(SO_4)(OH)$, metahohmannite, butlerite, parabutlerite, amarantite, hohmannite, and fibroferrite. *European Journal of Mineralogy*, **30**, 259–275.

Masquelier C. and Croguennec L. (2013) Polyanionic (phosphates, silicates, sulfates) frameworks as electrode materials for rechargeable Li (or Na) batteries. *Chemical Reviews*, **113**, 6552–6591.

Masquelier C., Reale P., Wurm C., Morcrette M., Dupont L. and Larcher D. (2002) Hydrated iron phosphates $FePO_4\cdot nH_2O$ and $Fe_4(P_2O_7)_3\cdot nH_2O$ as 3 V positive electrodes in rechargeable lithium batteries. *Journal of The Electrochemical Society*, **149**, A1037–A1044.

Masquelier C., Morcrette M., Reale P. and Wurm C. (2003) *Hydrated Iron Phosphate Electrode Materials for Rechargeable Lithium Battery Cell Systems*. US Patent: 2003/0064287 A1.

Mooney-Slater R.C.L. (1961) X-ray diffraction study of indium phosphate dihydrate and isostructural thallic compounds. *Acta Crystallographica*, **14**, 1140–1146.

Mooney-Slater R.C.L. (1966) The crystal structure of hydrated gallium phosphate of composition $GaPO_4\cdot 2H_2O$. *Acta Crystallographica*, **20**, 526–534.

Moore P.B. (1966) The crystal structure of metastrengite and its relationship to strengite and phosphophyllite. *American Mineralogist*, **51**, 168–176.

Nabar M.A. and Paralkar S.V. (1975) Thermal decomposition of some divalent metal selenates. *Thermochimica Acta*, **11**, 187–196.

Otwinowski Z., Borek D., Majewski W. and Minor W. (2003) Multiparametric scaling of diffraction intensities. *Acta Crystallographica*, **A59**, 228–234.

Padhi A.K., Nanjundaswamy K.S. and Goodenough J.B. (1997) Phospho-olivines as positive-electrode materials for rechargeable lithium batteries. *Journal of the Electrochemical Society*, **144**, 1188–1194.

Perchiazzi N., Ondruš P. and Skála R. (2004) Ab-initio X-ray powder structure determination of parascorodite, $Fe(H_2O)_2AsO_4$. *European Journal of Mineralogy*, **16**, 1003–1007.

Plášil J. (2018) Structural complexity of uranophane and uranophane-β: Implications for their formation and occurrence. *European Journal of Mineralogy*, **30**, 253–257.

Plášil J., Petříček V. and Majzlan J. (2017) A commensurately modulated structure of parabutlerite, $Fe^{III}SO_4(OH)\cdot 2H_2O$. *Acta Crystallographica*, **B73**, 856–862.

Robie R.A., Hemingway B.S. and Fisher J.R. (1979) Thermodynamic properties of minerals and related substances at 298.15 K and 1 bar (105 pascals) pressure and at higher temperatures. *U.S. Geological Survey Bulletin*, **1452**, 456 pp.

Ronis M. (1970) Chromium arsenate, $CrAsO_4$: preparation and study of two hydrates and of the anhydrous compound. *Comptes Rendus de l'Académie des Sciences, Série C*, **271**, 64–66 [in French].

Ronis M. and D'Yvoire F. (1974) Trivalent metal arsenates. III. Preparation and study of the stoichiometric dihydrates $MAsO_4.2H_2O$ (M = aluminum, gallium, chromium, iron) and the nonstoichiometric dihydrates $M_{1-x}H_{3x}AsO_4.2H_2O$. *Bulletin de la Société Chimique de France*, **1974**, 78–82 [in French].

Salvador Salvador P. and Fayos J. (1972) Structural relation between "Messbach-type" and "Lucin-type" variscites. *American Mineralogist*, **57**, 36–44.

Schindler M., Joswig W. and Baur W.H. (1995) Preparation and crystal structures of the vanadium phosphates $VPO_4\cdot 2H_2O$ and $V_{5.12}(PO_4)_4(OH)_{3.36}(H_2O)_{0.64}\cdot 0.84H_2O$. *European Journal of Solid State and Inorganic Chemistry*, **32**, 109–120.

Schroffenegger M., Eder F., Weil M., Stöger B., Schwendtner K. and Kolitsch U. (2020) News about thallium arsenates(V). *Journal of Alloys and Compounds*, **820**, 153369.

Schwendtner K. and Kolitsch U. (2007*a*) Gittinsite-type M^{1+}-M^{3+}-diarsenates (M^{1+} = Li, Na; M^{3+} = Al, Sc, Ga): insights into an unexpected isotypy and crystal chemistry of diarsenates. *Mineralogical Magazine*, **71**, 249–263.

Schwendtner K. and Kolitsch U. (2007*b*) Two new structure types: $KFe_3(AsO_4)_2(HAsO_4)_2$ and $K(H_2O)M^{3+}(H_{1.5}AsO_4)_2(H_2AsO_4)$ (M^{3+} = Fe, Ga, In) – synthesis, crystal structure and spectroscopy. *European Journal of Mineralogy*, **19**, 399–409.

Schwendtner K. and Kolitsch U. (2017) $M\mathrm{In}(HAsO_4)_2$ (M = K, Rb, Cs): three new hydrogenarsenates adopting two different structure types. *Acta Crystallographica*, **E73**, 1580–1586.

Schwendtner K. and Kolitsch U. (2018) $(NH_4)Ga(HAsO_4)_2$ and $TlAl(HAsO_4)_2$ – two new $RbFe(HPO_4)_2$-type M^+M^{3+} arsenates. *Acta Crystallographica*, **E74**, 1504–1508.

Serezhkin V.N., Kryuchkova G.V. and Kazakevich V.S. (2003) Coordination polyhedra ScX_n (X = O, S, Se, Te) in crystal structures. *Zhurnal Neorganicheskoi Khimii*, **48**, 1322–1330 [in Russian].

Sergeeva A.V. (2016) To the question of variscite and metavariscite formation. Phase equilibria in the system Al_2O_3–H_2O–P_2O_5. *Zapiski Rossiiskogo Mineralogicheskogo Obshchestva*, **145**, 101–113 [in Russian].

Shannon R.D. (1976) Revised effective ionic radii and systematic studies of interatomic distances in halides and chalcogenides. *Acta Crystallographica*, **A32**, 751–767.

Sheldrick G.M. (2002) *SADABS Area-Detector Absorption Correction Program*. Bruker AXS Inc., Madison, Wisconsin.

https://doi.org/10.1180/mgm.2020.57 Published online by Cambridge University Press

Sheldrick G.M. (2008) A short history of *SHELX*. *Acta Crystallographica*, **A64**, 112–122.

Sheldrick G.M. (2015) Crystal structure refinement with *SHELXL*. *Acta Crystallographica*, **C71**, 3–8.

Smith J.V. (1977) Enumeration of 4-connected 3-dimensional nets and classification of framework silicates. I. Perpendicular linkage from simple hexagonal net. *American Mineralogist*, **62**, 703–709.

Snyman H.C. and Pistorius C.W.F.T. (1963) Crystallographic data for $NiSeO_4$ and its hydrates. *Zeitschrift für Anorganische und Allgemeine Chemie*, **324**, 157–161.

Song Y., Yang S., Zavalij P.Y. and Whittingham M.S. (2002*a*) Temperature-dependent properties of $FePO_4$ cathode materials. *Materials Research Bulletin*, **37**, 1249–1257.

Song Y., Zavalij P.Y., Suzuki M., Whittingham M.S. (2002*b*) New iron(III) phosphate phases: crystal structure and electrochemical and magnetic properties. *Inorganic Chemistry*, **41**, 5778–5786.

Spencer E.C., Soghomonian V. and Ross N.L. (2015) Gallium arsenate dihydrate under pressure: elastic properties, compression mechanism, and hydrogen bonding. *Inorganic Chemistry*, **54**, 7548–7554.

Stoilova D. and Koleva V. (1995*a*) X-ray diffraction study on $MgSeO_4{\cdot}6H_2O$ at elevated temperatures. *Crystal Research and Technology*, **30**, 547–551.

Stoilova D. and Koleva V. (1995*b*) Thermal dehydration of magnesium selenate hydrates. *Thermochimica Acta*, **255**, 33–38.

Stoilova D. and Koleva V. (1997) TG, DTA, DSC and X-ray powder diffraction studies on some nickel selenate hydrates. *Thermochimica Acta*, **290**, 85–91.

Strunz H. and von Sztrokay K. (1939) Isodimorphie zwischen Metavariscit, Variscit, Phosphosiderit und Strengit. *Zentralblatt für Mineralogie und Geologie, Abteilung A*, **1939**, 272–278 [in German].

Sugiyama K., Yu J., Hiraga K. and Terasaki O. (1999) Monoclinic $InPO_4{\cdot}2H_2O$. *Acta Crystallographica*, **C55**, 279–281.

Tang X., Gentiletti M.J. and Lachgar A. (2002) Synthesis and crystal structure of indium arsenate and phosphate dihydrates with variscite and metavariscite structure types. *Journal of Chemical Crystallography*, **31**, 45–50.

Taxer K. and Bartl H. (2004) On the dimorphy between the variscite and clinovariscite group: refined finestructural relationship of strengite and clinostrengite, $Fe(PO_4){\cdot}2H_2O$. *Crystal Research and Technology*, **39**, 1080–1088.

Wells A.F. (1954) The geometrical basis of crystal chemistry. Part 2. *Acta Crystallographica*, **7**, 545–554.

Wilk H. (1959) Phosphosiderit und Strengit von Pleystein in Ostbayern. *Acta Albertina Ratisbonensia*, **23**, 107–170 [in German].

Woods T.L. and Garrels R.M. (1987) *Thermodynamic Values at Low Temperature for Natural Inorganic Materials: An Uncritical Survey*. Oxford University Press, New York–Oxford, 242 pp.

Xu Y Koh L.L., An L.H., Xu R.R. and Qiu S.L. (1995) A comparative study of a novel microporous indium phosphate and other $M(III)X(V)O_4$-type microporous materials. *Journal of Solid State Chemistry*, **117**, 373–378.

Xu Y., Zhou G.-P. and Zheng X.-F. (2007) Redetermination of iron(III) arsenate dihydrate. *Acta Crystallographica*, **E63**, i67–i69.

Yang H., Li C., Jenkins R.A., Downs R.T. and Costin G. (2007) Kolbeckite, $ScPO_4{\cdot}2H_2O$, isomorphous with metavariscite. *Acta Crystallographica*, **C63**, i91–i92.

Zaitsev A.N., Zhitova E.S., Spratt J., Zolotarev A.A. and Krivovichev S.V. (2017) Isolueshite, $NaNbO_3$, from the Kovdor carbonatite, Kola peninsula, Russia: Composition, crystal structure and possible formation scenarios. *Neues Jahrbuch für Mineralogie, Abhandlungen*, **194**, 165–173.

Zoppi M. and Pratesi G. (2009) Rietveld refinement of a natural cobaltian mansfieldite from synchrotron data. *Acta Crystallographica*, **E65**, i6–i7.

https://doi.org/10.1180/mgm.2020.57 Published online by Cambridge University Press